



OPEN ACCESS

Rubin Observatory LSST Stars Milky Way and Local Volume Star Clusters Roadmap

Christopher Usher¹ , Kristen C. Dage² , Léo Girardi³ , Pauline Barmby⁴ , Charles J. Bonatto^{5,6} , Ana L. Chies-Santos^{5,6} , William I. Clarkson⁷ , Matias Gómez Camus⁸ , Eduardo A. Hartmann^{5,6} , Annette M. N. Ferguson⁹ , Adriano Pieres⁶ , Loredana Prisinzano¹⁰ , Katherine L. Rhode¹¹ , R. Michael Rich¹² , Vincenzo Ripepi¹³ , Basilio Santiago^{5,6} , Keivan G. Stassun¹⁴ , R. A. Street¹⁵ , Róbert Szabó^{16,17} , Laura Venuti¹⁸ , Simone Zaggia³ , Marco Canossa^{5,6} , Pedro Floriano^{5,6} , Pedro Lopes^{5,6} , Nicole L. Miranda^{5,6} , Raphael A. P. Oliveira^{6,19} , Marta Reina-Campos^{20,21} , A. Roman-Lopes²² , and Jennifer Sobeck²³

¹ The Oskar Klein Centre, Department of Astronomy, Stockholm University, AlbaNova, SE-10691 Stockholm, Sweden

² Department of Physics, McGill University, 3600 University Street, Montréal, QC H3A 2T8, Canada

³ INAF—Osservatorio Astronomico di Padova, Vicolo dell’Osservatorio 5, I-35122 Padova, Italy

⁴ Dept of Physics & Astronomy and Institute for Earth & Space Exploration, University of Western Ontario, London, Canada

⁵ Instituto de Física, Universidade Federal do Rio Grande do Sul (UFRGS), Porto Alegre, RS, Brazil

⁶ Laboratório Interinstitucional de e-Astronomia—LineA, Rua Gal. José Cristino 77, Rio de Janeiro, RJ—20921-400, Brazil

⁷ Natural Sciences Department, University of Michigan-Dearborn, 4901 Evergreen Road, Dearborn, MI 48128, USA

⁸ Instituto de Astrofísica, Universidad Andres Bello, Fernandez Concha 700, Las Condes, Santiago, Chile

⁹ Institute for Astronomy, University of Edinburgh Royal Observatory, Blackford Hill, Edinburgh EH9 3HJ, UK

¹⁰ INAF—Osservatorio Astronomico di Palermo, Piazza del Parlamento, 1 I-90129 Palermo, Italy

¹¹ Department of Astronomy, Indiana University, Bloomington, IN 47405, USA

¹² Department of Physics and Astronomy, UCLA, PAB 430 Portola Plaza, Los Angeles, CA 90095-1547, USA

¹³ INAF—Osservatorio Astronomico di Capodimonte, Salita Moiariello 16, I-80131, Napoli, Italy

¹⁴ Department of Physics and Astronomy, Vanderbilt University, Nashville, TN 37235, USA

¹⁵ Las Cumbres Observatory, 6740 Cortona Drive, Suite 102, Goleta, CA 93117, USA

¹⁶ Konkoly Observatory, CSFK, MTA Centre of Excellence, H-1121 Konkoly Thege Miklós út 15-17, Budapest, Hungary

¹⁷ MTA CSFK Lendület Near-Field Cosmology Research Group H-1121 Konkoly Thege Miklós út 15-17, Budapest, Hungary

¹⁸ SETI Institute, 339 Bernardo Ave, Suite 200, Mountain View, CA 94043, USA

¹⁹ Universidade de São Paulo, IAG, Rua do Matão 1226, São Paulo 05508-090, Brazil

²⁰ Department of Physics & Astronomy, McMaster University, 1280 Main Street West, Hamilton, L8S 4M1, Canada

²¹ Canadian Institute for Theoretical Astrophysics (CITA), University of Toronto, 60 St George St, Toronto, M5S 3H8, Canada

²² Department of Astronomy—Universidad de La Serena, Chile

²³ Canada-France-Hawaii Telescope, 65-1238 Mamalahoa Hwy, Waimea, HI 96743, USA

Received 2023 May 22; accepted 2023 July 4; published 2023 July 20

Abstract

The Vera C. Rubin Observatory will undertake the Legacy Survey of Space and Time, providing an unprecedented, volume-limited catalog of star clusters in the Southern Sky, including Galactic and extragalactic star clusters. The Star Clusters subgroup of the Stars, Milky Way and Local Volume Working Group has identified key areas where Rubin Observatory will enable significant progress in star cluster research. This roadmap represents our science cases and preparation for studies of all kinds of star clusters from the Milky Way out to distances of tens of megaparsecs.

Key words: Globular star clusters – Surveys

1. Introduction

The Vera C. Rubin Observatory is currently under construction on Cerro Pachón in Chile. Over the course of ten years, the Rubin Observatory will carry out the Legacy Survey of Space and Time (LSST, Ivezić et al. 2019), imaging 18,000 square degrees of the southern sky over 760 times (and a further 9000 square degrees at

least 120 times as per the `baseline_v3.0_10yrs` Opsim run; Delgado et al. 2014) in six optical filters (*ugrizy*). With a median 5σ point source depth of $r = 24$ per visit and median co-added depth of $r = 26.9$ (in the wide fast deep survey area as per the `baseline_v3.0_10yrs` Opsim run) as well as a median effective seeing of $1''.0$, LSST will provide deep, high-quality imaging over an unprecedented area.

Rubin/LSST Science Collaborations are independent federations of worldwide communities of scientists, self organized based on their interests and expertise. They are built primarily to prepare for LSST observations—e.g., by providing expert

Original content from this work may be used under the terms of the [Creative Commons Attribution 3.0 licence](https://creativecommons.org/licenses/by/3.0/). Any further distribution of this work must maintain attribution to the author(s) and the title of the work, journal citation and DOI.

advice and analysis to Rubin; by training, educating and engaging the scientific community; and by carrying out other activities such as fund-raising, software development, and implementing research inclusion practices. The Star Clusters Science Working Group (SCSWG) was recreated in 2022 inside the Stars, Milky Way and Local Volume (SMWLV) collaboration to promote these activities in regards to star clusters. While firmly based on the SMWLV collaboration, this working group has strong connections with the Galaxies and the Transients and Variable Stars Science Collaborations.

Star clusters, both within our own galaxy and beyond, are a window onto a wide range of astrophysical processes, including the following questions:

1. How do stars form, evolve and die?
2. How do star clusters form, evolve and dissolve?
3. How do galaxies form and evolve?
4. What is the dark matter content of galaxies?

LSST will allow us to observe the nearest open clusters at distances of less than 100 pc and the most massive globular clusters out to a redshift of $z=0.06$ with the same survey. Studying both Galactic and extragalactic star clusters in the same survey is complementary in terms of the scientific goals that can be achieved. Star clusters in our own Galaxy can be studied in much greater detail than extragalactic ones. Observations of extragalactic star clusters allow them to be studied in galaxies with a wide range of masses, morphologies and environments. This allows us to understand what features of the Milky Way's star clusters are universal and what varies.

Although this roadmap was prepared by the SMWLV Star Clusters working group, star cluster science extends beyond the SMWLV collaboration to encompass the interests of the Galaxies, Dark Energy and Transients and Variable Stars collaborations.

A bewildering range of terms including open clusters, globular clusters, young massive clusters, super star clusters, faint fuzzies (e.g., Brodie & Larsen 2002; Chies-Santos et al. 2013; Romanowsky et al. 2023), extended star clusters (e.g., Huxor et al. 2005; Bianchini et al. 2015), diffuse star clusters (e.g., Peng et al. 2006) and ultra compact dwarfs (e.g., Brüns & Kroupa 2012) are used to describe different populations of star clusters, with different parts of the community (i.e., Galactic versus extragalactic) using different terms to describe objects with similar physical properties.

The traditional distinction between old, metal-poor, massive and dense globular clusters in the halo and young, metal-rich, low mass and diffuse open clusters in the disk breaks down when we go other galaxies (and even in the Milky Way is partially due to observational biases). Many modern theories (e.g., Elmegreen & Efremov 1997; Kruijssen 2015) of star cluster formation posit a common origin for the diverse population star clusters we observe.

A distinction, however, should be made between non-nuclear star clusters and nuclear star clusters, since instead of being formed in a single burst of star formation, nuclear star clusters are built up through a combination of the in-spiral of massive star clusters via dynamical friction and in situ star formation over an extended period of time. A distinction should also be made between non-nuclear star clusters and objects such as ω Cen and M54, which are believed to be the stripped nuclei of accreted galaxies. We prefer the term candidate nuclear remnant (CNR) for these stripped objects to the more common term of ultra-compact dwarf (UCD), given that the observed population of UCDs contains a mix of massive or extended star clusters and NRs and that there is a lack of consensus about the definition of UCDs.

In this road map, we use the term young cluster to refer to star clusters with ages of a few hundred million years and younger and globular clusters for star clusters older than this. This young/old distinction is mostly between epochs dominated by cluster formation and dissolution processes, but in stellar evolution terms, it roughly corresponds to when the red giant branch starts to make a significant contribution to the star cluster's luminosity. Among the old clusters, we can also define the class of "intermediate-aged" clusters, which is useful from the point of view of the theory of stellar populations: such clusters are characterized by the presence of stars with convective cores at the turn-off and an extended red giant branch (RGB). We note that most of the observational techniques used to identify and study star clusters, both resolved and unresolved, are similar for young and old star clusters.

2. Milky Way Star Clusters

Star clusters in the Milky Way are fundamental for the calibration of stellar evolution and stellar population models, and serve as important probes of the formation history of the Galaxy. Their study has significantly improved since the availability of Gaia proper motions and parallaxes (see Cantat-Gaudin 2022, for a review), which provided more reliable distances, orbital information, membership probabilities and a number of new candidate clusters. The significantly deeper time-series photometry from LSST will likely allow us to extend the Gaia revolution, with a more complete sampling of the fainter stellar members, and of more distant or extincted star clusters. By combining Gaia and LSST photometry/astrometry, it will be possible to catalog more distant members and to associate stellar streams with clusters. Thanks to its high resolution and multicolor photometry, LSST has the prospect of identifying new clusters in the Galactic plane. In fields too extinct or dense for Gaia, LSST will provide the astrometry that will enable cluster members to be separated from the field. If deep enough, u -band photometry will prove crucial in disentangling multiple populations.

2.1. Which MW Clusters will LSST Observe, and to which Depth?

With the optimization of LSST cadence and footprint being well advanced (see Bianco et al. 2022), now we have a close-to-final idea of which MW clusters will be observed, and to which depth. This, has been evaluated for the baseline plan baseline_v2.1_10yrs, in the following way:

1. We create a combined list of Galactic globular clusters (GGC) from the Baumgardt & Vasiliev (2021) and Harris (1996) catalogs. It contains 160 objects.
2. We eliminate the GGCs from the Kharchenko et al. (2013) catalog, producing a clean list of open clusters (OCs) with 2862 objects. Although not reflecting the more complete census of MW star clusters provided by the latest Gaia data releases (see e.g., Cantat-Gaudin et al. 2018; Castro-Ginard et al. 2020; Kounkel et al. 2020; Cantat-Gaudin 2022; Hao et al. 2022; Hunt & Reffert 2023), Kharchenko et al. (2013)’s catalog still provides essentially the same distribution in terms of distances and ages.
3. In the metrics analysis facility (MAF; Jones et al. 2014), we provide their central coordinates to `maf.UserPointsSlicer` and evaluate a series of metric values, comprising `maf.Coaddm5Metric()` and `maf.CrowdingM5Metric(crowding_error=0.25)` (hereafter `CoaddM5` and `CrowdingM5`, for short), for all 6 LSST filters.

Already at this stage,²⁴ only clusters inside the footprint –totalling 144 GGCs and 2022 OCs–provide valid metric values. About 2/3 of these GGCs are found in the main wide fast footprint, the others being in the Galactic Plane minisurvey. For OCs, these fractions reverse, with $\sim 1/3$ of the OCs centers being in the WFD footprint. Curiously, there is one GGC in a deep drilling field (namely the remote Arp-Madore 1 cluster, in the Euclid deep drilling field).

The above-mentioned `CoaddM5` and `CrowdingM5` metrics represent, respectively, the 5σ limit for stellar photometric detections, and the limit at which photometric errors induced by crowding (due to the foreground/background MW populations) start causing severe incompleteness (above $\sim 50\%$; see W. Clarkson et al. 2023, in preparation). Therefore, the minimum between these two limits, for every filter λ , provides the faintest stars to be measured in the clusters:

$$m_\lambda = \min(\text{CoaddM5}_\lambda, \text{CrowdingM5}_\lambda). \quad (1)$$

For GGCs, this limit is valid only in the cluster outskirts, since their inner regions will be affected by additional “self-

crowding.” Using the cluster tabulated distances and extinctions, we can also derive the maximum depth in absolute magnitudes, M_λ :

$$M_\lambda = m_\lambda - \mu_0 - E_\lambda \times A_V \quad (2)$$

where μ_0 is the true distance modulus and E_λ is the ratio between the extinction in every filter and the extinction in the V band, A_V . E_λ values are taken from Chen et al. (2019).

All the m_λ and M_λ values are plotted in Figures 1 and 2 against some of the main cluster properties listed in the original catalogs, namely [Fe/H] for GGCs and $\log(\text{age}[\text{yr}])$ for OCs. Several aspects are evident in these plots:

1. m_λ values concentrate into two narrow strips close to the 25th–27th magnitude limits (depending on the filter). These two strips reflect the `CoaddM5` limit in uncrowded regions of the MW for the two possible numbers of visits (either ~ 810 in the main WFD footprint, or ~ 250 in the Galactic Plane mini-survey).
2. There is an extended distribution of m_λ to brighter values, as low as ~ 20 mag. These points reflect the `CrowdingM5` limit in very crowded areas of the MW.
3. Irrespective of their concentration/distribution in different m_λ intervals, the clusters are well distributed in their intervals of [Fe/H] and $\log(\text{age})$;
4. The distributions in M_λ appear quite promising, with significant numbers of clusters being sampled down to absolute magnitudes of $\gtrsim 10$, for both OCs and GGCs.
5. Even more interesting is that significant numbers of OCs (of all ages) will be sampled to absolute magnitudes exceeding 15 (and even reaching 20 mag).

These latter points emphasize one of the greatest promises of LSST regarding star clusters: to sample faint features that have not been clearly documented in clusters of known age and metallicity, either by Gaia or by previous deep photometric surveys. We recall that the majority of the sample of field white dwarfs (WD) observed by Gaia starts at $M_G \gtrsim 10$ and suddenly bifurcates at $M_G \gtrsim 12$ (corresponding to $M_u \gtrsim 10$; see Gaia Collaboration et al. 2018)—however Gaia did not observe WDs in clusters with $M_G \gtrsim 13$. Moreover, we recall that the $15 < M_i < 20$ interval already corresponds to substellar objects, i.e., brown dwarfs.

2.2. Finding New MW Clusters with LSST

With unprecedented depth and homogeneous coverage, LSST will resolve main sequence low-mass stars in clusters belonging to disk and halo of the MW, and stars at the top of the AGB belonging to the typical population of old and metal-poor star clusters out to $m - M \sim 28$ or 4 Mpc, assuming a range of magnitude equal to 1 magnitude below the brightest star in the AGB/RGB and a limiting magnitude equal to $g = 27$. Despite the effect of crowding in the center of very

²⁴ See the current working version of the cluster list at the url https://drive.google.com/drive/folders/1p1p1btLV4iUJamU1bu_UgFA5aKDePBXB?usp=sharing. The list will be updated by the SCSWG according to the latest baseline plans and available cluster catalogs.

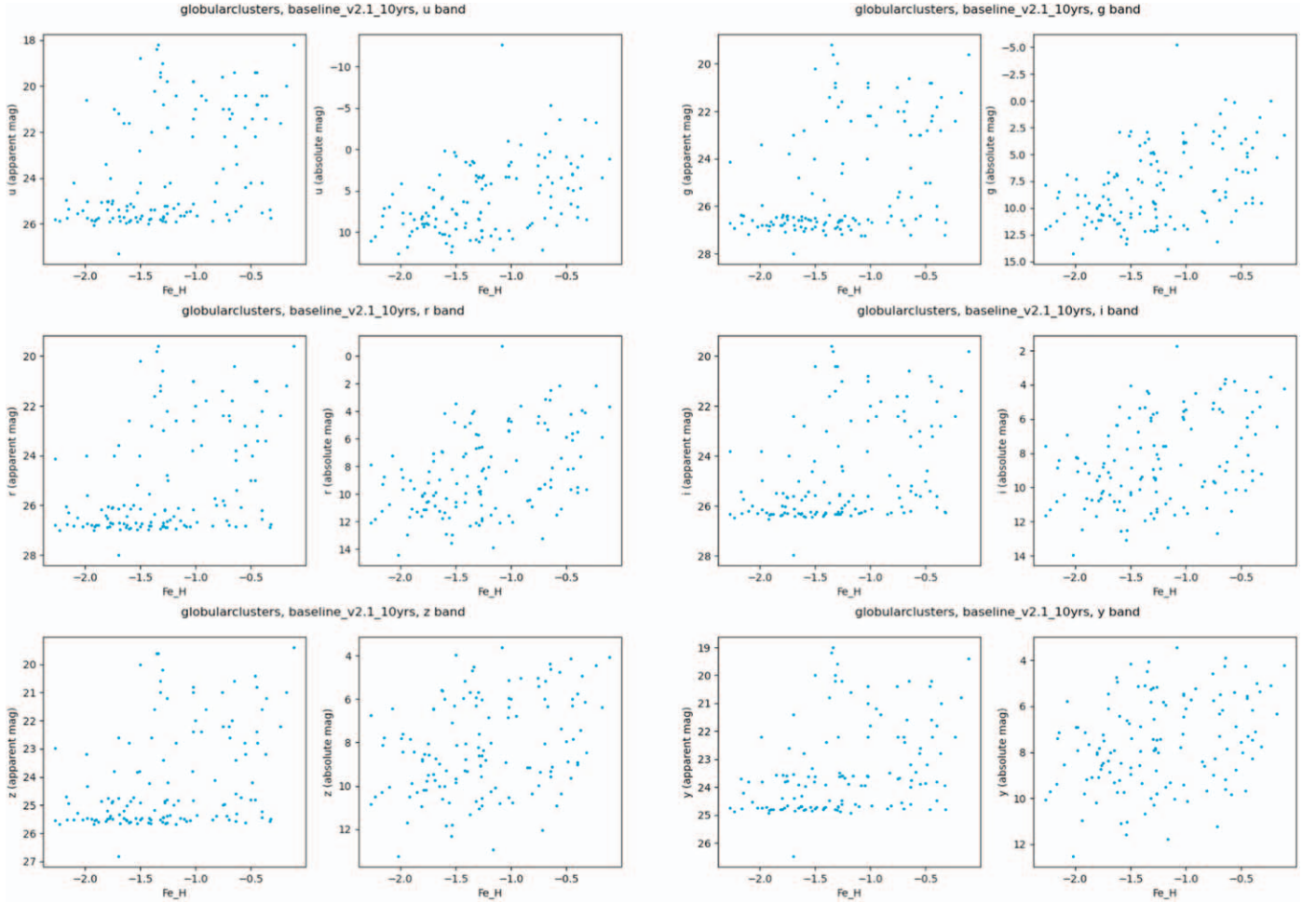


Figure 1. Maximum photometric depths to be reached in the outskirts of known MW GGCs, according to Equations (1) and (2) and assuming `baseline_v2.1_10yrs`. Results are presented for all LSST filters, in AB mags, as a function of $[\text{Fe}/\text{H}]$.

distant objects, this will allow for a complete census of faint halo clusters and dwarf galaxies in the entire southern hemisphere in the large vicinity of the MW. LSST will also provide astrometric measurements to four magnitudes fainter than provided by Gaia (see Section 3.7 of LSST Science Collaboration et al. 2009). Methods for identifying new clusters and associations through the combination of photometry, parallaxes, and proper motions have recently been demonstrated by Kounkel et al. (2020), who also have extended the technique to very large samples with the application of machine learning (McBride et al. 2021; Prisinzano et al. 2022). A few other methods have been refined using recent Gaia data releases, as nicely summarized in Hunt & Reffert (2021, 2023).

The resulting data will offer crucial insights into the interaction between the Galaxy and the nearest dwarf galaxies, such as the Magellanic Clouds, as well as the interactions among the dwarf galaxies themselves (see for instance Deason

et al. 2015; Jethwa et al. 2016) and its group of satellites (Patel et al. 2020). This information will improve our understanding of the behavior of external star clusters along the interactions, and help determine the original host galaxy of the star cluster (see for instance Mau et al. 2019 and references therein). Additionally, the data will provide clues about the evolution of galaxies and help to evaluate the bottom-up scenario for the formation of galaxies in the Λ -CDM model (Bullock & Johnston 2005).

However, detecting star clusters in LSST presents a challenge due to the amount of data that will be produced. An estimation of about one billion stars down to $g = 27$ is very realistic (see, e.g., Dal Tio et al. 2022), without accounting for galaxy/QSO contamination and regions very close to the Galactic plane, while using typical limits in color for expected stellar evolutionary phases in old and metal-poor systems (MS, RGB, AGB, and HB stars). Typically, in order to detect star clusters a

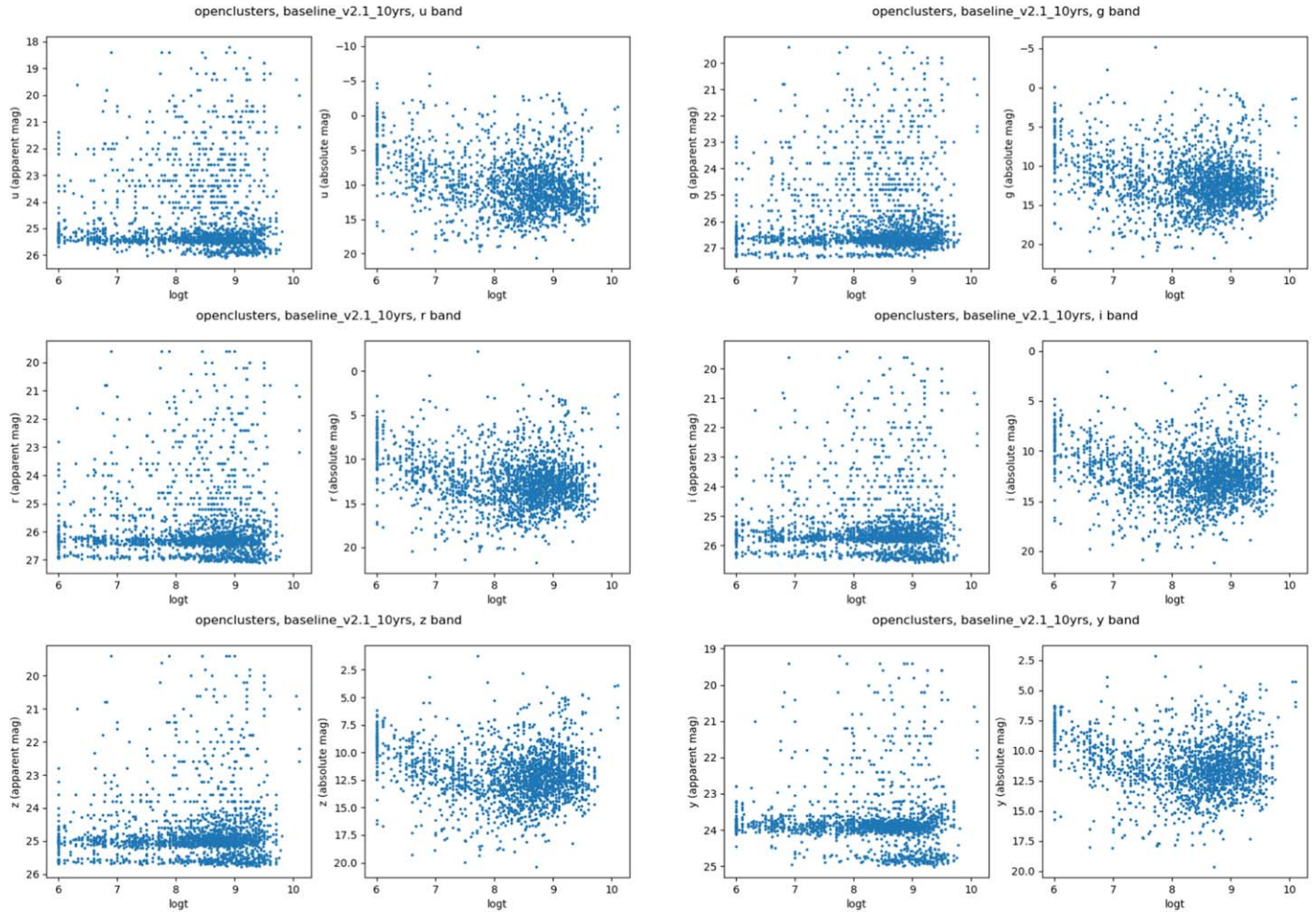


Figure 2. The same as in Figure 1, but for OCs as a function of $\log(\text{age}/\text{yr})$.

matched filter is applied to the data sample (see for instance Balbinot et al. 2013; Bechtol et al. 2015 and Koposov et al. 2015), selecting stars belonging to a specific stellar population at a specific distance. Local peaks in the stellar population are then detected, and a list of candidates is generated, which is subsequently analyzed and duplicates removed, among other steps. In LSST, we expect to read positions, as well as magnitudes in the g and r filters and their respective photometric errors. We note that the situation is somewhat different in current Gaia-based searches for new clusters (e.g., Castro-Ginard et al. 2020; Hunt & Reffert 2023), which very much rely on the measured proper motions—although the problems related with the huge amount of data are essentially the same.

To handle this vast amount of data, the search for stellar clusters in the vicinity of the MW must leverage computational expertise and run searches in multiple regions and distances simultaneously to provide results within a reasonable time (in the worst case, a very few days).

Tests are currently underway with a pipeline based on detections of clusters of galaxies (Aguena et al. 2021), which selects stars based on old and metal-poor isochronal masks at specific distances to detect both dwarf galaxies and faint halo clusters in the Local Volume. Codes have been developed to create simulations based on LSST’s photometric system and depth, inserting stellar clusters in a MW foreground of stars. After simulating an area of the sky, the code detects the candidates, running many regions in parallel and concatenating the list of detections into a single catalog that includes parameters such as position, signal-to-noise ratio, size, and distance.

2.3. Young Open Clusters, Moving Groups, and Associations

Very young open clusters, which span the range of ages relevant to protoplanetary disk lifetimes ($<10\text{--}20$ Myr; e.g., Ribas et al. 2014), allow us to probe a key stage in early stellar

evolution. At these young ages, the dynamics of young, low-mass stars are governed by the interaction with their surrounding disks. This star–disk connection regulates the accretion of mass from the disk to the star (e.g., Hartmann et al. 2016) and the shedding of angular momentum at the disk–magnetosphere interface (e.g., Ireland et al. 2021), and has a long-lasting impact on the fundamental properties of the final star. In addition, local changes in density and structure that are triggered by the accretion flow across the inner disk can reverberate on the migration pattern of close-in planets, impacting how these settle onto their final orbits (Liu et al. 2017; Romanova et al. 2019).

The physical parameters of the youngest pre-main sequence (PMS) stars (e.g., spectral type, radius, magnetic field configuration, mass accretion rate \dot{M}_{acc}) are often difficult to measure precisely over a broad range of stellar masses and ages, due to a mix of spatially variable reddening and nebular emission from H II regions, observational uncertainties, and model systematics (e.g., Hillenbrand & White 2004). As a result, detailed studies of star formation and early evolution have historically been restricted to relatively nearby open clusters and star-forming regions ($\lesssim 0.5\text{--}1$ kpc; e.g., Luhman 2012), with complete membership censuses from the highest to the lowest masses (spectral classes \sim B to L) limited to the closest stellar associations and moving groups ($\lesssim 0.1$ kpc; e.g., Bell et al. 2017). Over the last few years, significant progress has been achieved in cataloging all clustered young stellar populations within a distance of $\sim 1.5\text{--}2$ kpc, thanks to the synergy between accurate Gaia astrometric data and unsupervised machine learning algorithms (Prisinzano et al. 2022, and references therein). However, comprehensive determinations of individual stellar properties are required in order to capitalize on these results and build a uniform picture of star formation history and kinematics across our Galaxy. Thanks to the combination of deep sky mapping, multi-wavelength characterization, and long-term observational baselines, Rubin LSST will allow us to address many of these issues with unprecedented accuracy.

For example, it is now possible to empirically measure the radii of stars through the combination of broadband spectral energy distributions, providing the stars’ bolometric fluxes, together with parallaxes from Gaia and/or from Rubin itself, via the technique of “pseudo-interferometry” (see, e.g., Stassun & Torres 2016; Stassun et al. 2017). In addition, when spectroscopic surface gravity measurements are available, it is then also possible to measure the stellar masses as well (e.g., Stassun et al. 2018). The ability to measure stellar radii and masses in this way opens the prospect of LSST as an unprecedented factory for the determination of fundamental physical properties of stars with known ages by the tens of thousands (Stassun et al. 2018).

Studying the dynamics of disk accretion in young stellar objects is best done in the ultraviolet (UV) regime, which is sensitive to the energetic emission released by surface shocks that form at the location where magnetically channeled material from the disk is transferred to the star at near freefall velocities (Calvet & Gullbring 1998). The photometric U -band (or u -band) provides an effective tracer of the excess emission driven by accretion shocks on top of the stellar photosphere (Gullbring et al. 1998), and when combined with optical photometry, it can be used to define accretion-sensitive color indices that can be converted to instantaneous measurements of the total accretion luminosity and \dot{M}_{acc} (e.g., Rigliaco et al. 2011; Venuti et al. 2014; Kalari et al. 2015). The contemporaneous availability of multiple UV-optical filters is critical for a proper estimation of stellar and accretion parameters (e.g., Stassun & Wood 1999; Venuti et al. 2021), especially for disentangling the flux contribution due to accretion, the stellar activity component, and the effect of interstellar extinction (e.g., Bouvier et al. 1993; Vrba et al. 1993; Venuti et al. 2015).

Key questions regarding the star–disk interaction stage of PMS evolution include for how long disk accretion persists, how the pattern of disk accretion is influenced by stellar properties such as mass and metallicity, and what connects routine, low-level accretion ($\dot{M}_{\text{acc}} \sim 10^{-8} M_{\odot} \text{ yr}^{-1}$ around solar-type stars) to eruptive accretion events where \dot{M}_{acc} can increase by 2–3 orders of magnitude (Fischer et al. 2022). Answers to these questions have significant implications for the angular momentum evolution of young stars, specifically setting the timescales of interest for interconnected mechanisms such as stellar winds and mass ejection (Bouvier et al. 2014). With an assumed Wide-Fast-Deep coverage of the Galactic plane and the many star-forming regions it encompasses (Prisinzano et al. 2023), Rubin LSST will have a transformative impact on these issues, by enabling simultaneous u , g , r , i detection of young ($\sim 1\text{--}10$ Myr) stars with relatively low extinction down to masses $\sim 0.1\text{--}0.2 M_{\odot}$ (spectral types \sim M5–M4) to distances of up to a few kpc. This is illustrated in the left panel of Figure 3, which represents the maximum distance that can be reached for a given limiting magnitude as a function of stellar age, stellar mass, and reddening, as presented in Damiani (2018).

A detailed analysis of the maximum distances that can be reached for a 10 Myr old star of $0.3 M_{\odot}$, by adopting four different Rubin Opsims, including the case with the Wide-Fast-Deep cadence extended to the Galactic Plane, is reported in Prisinzano et al. (2023, see their Figure 5). Rubin LSST simulations adopting their metric show that, with the deepest cadences, distances up to 9–14 kpc can be achieved. Such limits depend on the stellar ages, masses and reddening but are also strongly affected by the crowding effects.

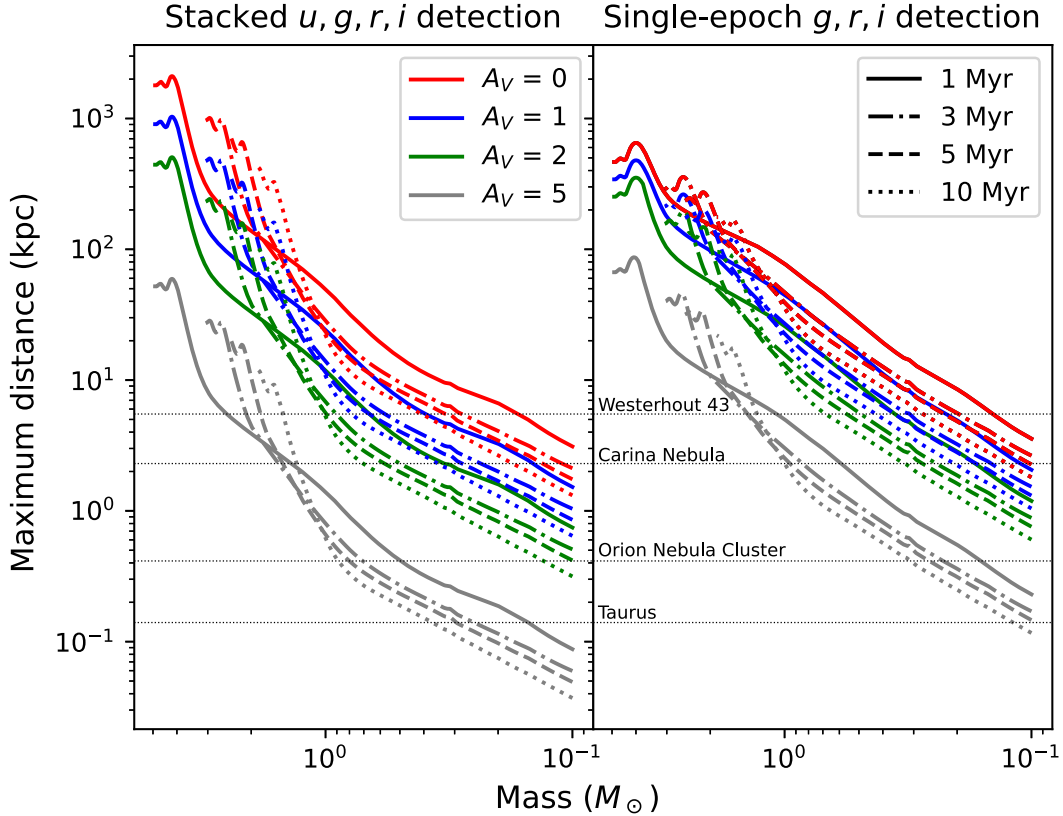


Figure 3. Projected maximum distance up to which young, PMS stars of different mass are expected to be detected in all of the u, g, r, i filters at the end of the 10 yr Rubin LSST survey (left panel), and in a single visit in g, r, i filters (right panel), as a function of age (different line styles) and reddening (different colors; see legend). The distances to some well-known star-forming regions are marked on the diagrams as a reference for the scale. These projections were derived by assuming the single-image and coadded-image 5σ depths simulated for the baseline survey (Bianco et al. 2022), and converting them to expected limiting distances by using the MIST isochrones (Choi et al. 2016; Dotter 2016) with synthetic LSST photometry, and a sample range of ages and extinction values.

The extent and depth of this sky mapping will allow uniform, quantitative measurements of the prevalence and strength of accretion activity for PMS stars of varying mass and age in different environments than the Solar neighborhood. When limiting the selection to the optical g, r, i filters, young, late-type M-stars are expected to be detected down to distances of a few kpc in a single visit (Figure 3, right), and up to a factor 3–4 deeper in the final coadded stack at the end of the survey. For intermediate-distance regions, this combination of depth and multi-wavelength information will enable cluster memberships to be refined down to the lowest masses; this is essential for accurate reconstructions of the stellar initial mass function (IMF) and to test its universality (Offner et al. 2014). At distances $>1\text{--}2$ kpc, the homogeneous detection of M-type stars will provide an invaluable tool to statistically identify and characterize new clustered PMS populations, by taking advantage of the peculiar color properties of M-dwarfs in g, r, i filters (Damiani 2018; Prisinzano et al. 2018; Venuti et al. 2019) and of the brightness contrast between young, M-type

PMS stars and more evolved M-type field dwarfs (e.g., Siess et al. 2000).

The peculiar color properties of M-dwarfs, which represent more than 80% of stellar cluster members (Lada 2006), also allow us to estimate individual reddening values. These are crucial to derive effective temperatures and stellar luminosities and then stellar ages by comparing them with stellar isochrones in the HR diagram. In turn, this enables analyzing the age distributions of stars in young clusters, which is necessary to address the still-unresolved question of the age spread and to impose strong constraints on the physical mechanisms and timescales involved in the process of cluster formation (e.g., Tassis & Mouschovias 2004; Palla et al. 2005; Ballesteros-Paredes et al. 2007).

While typical changes in the young star–inner disk environment are triggered on comparable or shorter timescales (days to weeks) than the expected observing cadence for LSST fields (e.g., Costigan et al. 2014; Flaischlen et al. 2022), the long observational baseline over which young open clusters and star-forming regions will be regularly sampled will be

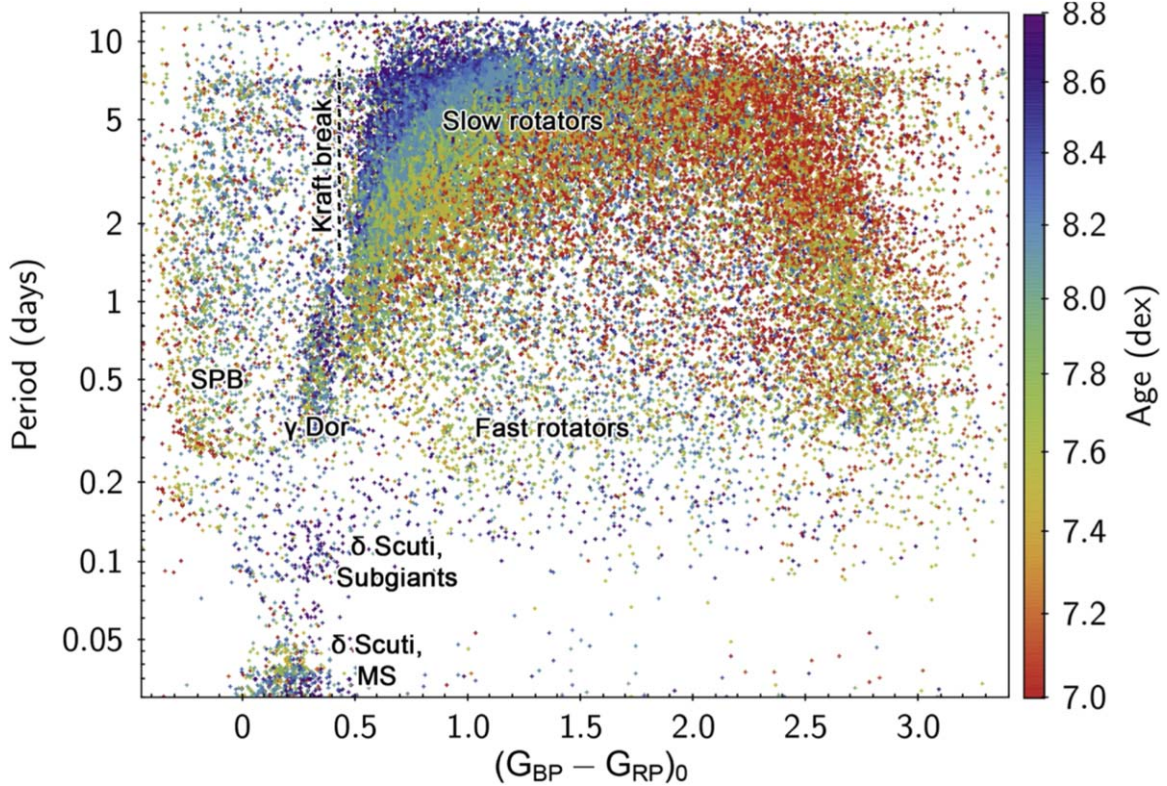


Figure 4. Recovered distribution of periods of the stars in the sample as a function of Gaia color, extinction-corrected, color-coded by their age, annotated with the features of the parameter space. Sources redder than the labeled “Kraft break” have the dominant mode of variability being caused by rotation. They can be separated into slow rotators (sources that show a clear evolution of their periods with age), and fast rotators, having typical periods < 1 day. Sources bluer than the Kraft break are commonly pulsators. γ Dor sources have pulsation frequency comparable to the stellar rotation period, consisting only of the main-sequence stars. δ Scuti stars in the age-limited sample form a bimodal distribution, with the main-sequence δ Scuti variables having periods shorter than 1.2 hr, and the subgiants having periods longer than 2 hr. Slowly pulsating B-type variables (SPB) are found among the early-type stars. Reproduced with permission from Kounkel et al. (2022). © The Author(s). Published by IOP Publishing Ltd. [CC BY 4.0](https://creativecommons.org/licenses/by/4.0/).

critical to assess the interplay between inner disk and outer disk dynamics, and to investigate the causal link between small-scale disk processes and large-scale eruptive behaviors that can develop over months to years (Bonito et al. 2023).

The homogeneous, multi-wavelength database that will be assembled over the entire Rubin LSST lifetime will also enable unprecedented evaluations of stellar magnetic cycles during the PMS phase, uniform measurements of stellar rotation rates, the identification of new PMS eclipsing binary systems in clusters (invaluable benchmarks for validating PMS evolutionary models; e.g., Gillen et al. 2020; Stassun et al. 2022), and potential detections of transiting substellar objects (e.g., Stassun et al. 2006). With regards to stellar rotation and the evolution of stellar angular momentum, recent work demonstrates the power of combining time-series photometry of large samples of young stars whose ages are known by virtue of their membership in clusters and associations (Kounkel et al. 2022, see Figure 4); LSST will dramatically expand the samples and more completely fill in the parameter space of stellar age, masses, and metallicity.

2.4. Star Clusters as Stellar Evolution Tools

Star clusters in the Milky Way that are fully resolved into stars are invaluable tools for calibrating stellar evolution models. The evolved stars within the clusters are expected to closely track theoretical isochrones in proportions that directly follow from the amount of time spent in different evolutionary phases, with only minimal dependence on the IMF. Particularly important in this regard are the intermediate-age star clusters, i.e., those old enough to develop an extended RGB sequence, but not old enough to be classified as ancient GGCs. Their main sequence turn-offs in the HR diagram display the characteristic hook caused by convective cores. They are also of primary importance for stellar population models, because they probe most of the history of our Galaxy, over the complete age range from ~ 1 to 8 Gyr.

The stars on the Main Sequence of such clusters have small convective cores, which brings a significant amount of uncertainty in the age-dating of the clusters. Indeed, stellar models with different amounts of convective core overshooting

may change the inferred ages by factors exceeding 50%. In addition, in recent years it has been recognized that the presence of fast rotators has a significant impact both in the definition of the “typical amount of convective overshooting” experienced by stars with all masses larger than $\sim 1.2M_{\odot}$ (Costa et al. 2019), and in the stars’ estimated ages. Indeed, rotation increases core masses and luminosities at the end of the main sequence in a way that partially mimics overshooting (see e.g., Ekström et al. 2012). A significant spread in rotational velocities causes main sequences with broad turn-offs at intermediate ages and split sequences in the youngest clusters (e.g., Kamann et al. 2020, 2023), but leaves no trace in the red giants, except for their increased core sizes and changes in the surface abundances of CNO elements. Their signature in color-color plots is tiny, although possibly detectable in star clusters with a very uniform reddening, and with a high fraction of fast rotators (Girardi et al. 2019).

Most of the present inferences regarding rotation derive from star clusters in the Magellanic Clouds (MCs), thanks to very precise Hubble Space Telescope (HST) photometry and large stellar populations in these objects. However, the study of rotation in the MCs is challenging given the difficulties in obtaining accurate spectroscopy in crowded clusters at >50 kpc distances. Fortunately, the phenomenon has also been identified in a few very nearby clusters (Brandt & Huang 2015; Cordoni et al. 2018; Gossage et al. 2018), and their characterization in other MW clusters might improve further with better membership information and dedicated spectroscopic studies. It is obvious that LSST will help to significantly expand the useful database of precise photometry and good memberships for these MW star clusters. In addition, the use of 6-band photometry is expected to produce much better extinction maps, hopefully further clarifying the features caused by fast rotators in the CMD.

Another controversial subject in recent years is the initial-to-final mass relation (IFMR) of stars in the $1\text{--}8 M_{\odot}$ interval. While this relation has been regarded as a close-to-linear relation with little dependence on metallicity (e.g., Weidemann 2000), claims have emerged of a significant non-monotonic behavior, or a kink, in the IFMR at near-solar metallicities (Cummings et al. 2018; Marigo et al. 2020). This may have significant implications for understanding the evolution of asymptotic giant branch (AGB) stars, which provide a fair fraction of the newly synthesized metals in galaxies, and of their near-infrared luminosities. Progress in this sense requires (1) a significant expansion in the detection and mass measurements of WDs in star clusters, and (2) eventually checking the mechanism that causes the kink using AGB stars in clusters (Marigo et al. 2022). Candidate AGB stars in MW clusters are presently very rare, and lack some relevant information such as their chemical types (roughly corresponding to the M/S/C spectral classification) and long-period variability. These are two areas in which the precise 6-band

time-series photometry of LSST, added to existing near-infrared photometry, will certainly produce some improvement.

Also important in these star clusters is the presence of products of close binary evolution, in particular the blue stragglers and hot subdwarfs, which form in a few subtypes and via (at least) a couple of channels whose relative importance are still not clear (see e.g., Heber 2009; Jadhav & Subramaniam 2021; Leiner & Geller 2021). Such stars are rare but the reliability of present catalogs has very much improved thanks to Gaia (Geier et al. 2019; Jadhav & Subramaniam 2021; Leiner & Geller 2021; Rain et al. 2021; Culpan et al. 2022). These types of stars are more easily detected in blue/UV filters, but the Galactic disk extinction is probably hiding a significant number of them from our view. The LSST deep u -band photometry in the near-disk region will be invaluable to increasing the size of the statistical sample in the MW.

Finally, double-lined eclipsing binaries (DLEBs) allow the precise determination of stellar masses and radii of their components, including for stars with known ages and representing alternate stellar evolution pathways such as red stragglers and others (see, e.g., Stassun et al. 2023). The few DLEBs presently known as cluster members indeed set strong constraints on the global properties of the host cluster, such as age and distance, and eventually on their initial helium content (e.g., Meibom et al. 2009; Thompson et al. 2010; Brogaard et al. 2021). LSST may significantly increase the numbers of known eclipsing binaries in clusters by factors of 1.7–3 (for globular clusters and open clusters, respectively; Geller et al. 2021), eventually leading to significant progress in this front.

2.5. Galactic Globular Clusters

Ninety percent of the known Milky Way globular clusters are located within the LSST footprint. As can be seen in Figure 1, LSST photometry will reach well below the main sequence turnoff at least in the outskirts of almost all of these GCs, while also reaching the hydrogen burning limit in a few clusters. So far, only Gaia provides a larger homogeneous sample of resolved star photometry in GCs, however LSST will reach five magnitudes deeper, and in six filters, as opposed to the 3 Gaia filters.

We have been able to learn a lot based on the photometric depth of HST’s dedicated surveys on Galactic GCs (e.g., Sarajedini et al. 2007; Nardiello et al. 2018). However, the coverage of the HST observations did not allow for wide field studies, encompassing the clusters as a whole. In contrast, the nearly all sky-coverage of LSST will provide a spatially comprehensive analysis of the Milky GC system, allowing us to study GCs from their central parts (dependent on crowding, etc.) to their outskirts. The largest homogeneous sample of wide-field photometry for GCs is from Stetson et al. (2019) which covers 48 GCs and makes use of a wide variety of instrumentation. In contrast, LSST will be homogeneous and

deeper. For inner halo GCs, Gaia has allowed detailed explorations of GC outskirts (e.g., de Boer et al. 2019; Sollima 2020; Kuzma et al. 2021). Indeed, as illustrated and quantified by Cantat-Gaudin et al. (2023), the Gaia catalogs become severely incomplete in the central parts of globular clusters.

The deep u -band photometry provided by LSST will allow the identification of N-rich stars and other features that can reveal multiple stellar populations in GCs. (e.g., Lardo et al. 2011). This can in turn be used to probe large scale radial variations and abundances in the different stellar populations of Galactic GCs. This is of foremost importance, as virtually all globular clusters studied in depth show evidence for multiple populations (see review by Bastian & Lardo 2018). It is worthwhile to note that the community has not yet reached a consensus as to what is the key driver for the appearance of multiple stellar populations in clusters. Moreover, it will be possible to look for N-rich giants outside of GCs and trace back field populations to previous generations of disrupted clusters (Martell et al. 2011; Schiavon et al. 2017).

Another important contribution will be on analyzing the outskirts of clusters and examining the properties of their extratidal stars and searching for evidence of tidal streams. LSST will enable the detection of even larger samples of stars than has been possible in the Gaia era (Bianchini et al. 2019; Ibata et al. 2019).

LSST will also enable a detailed study of variable phenomena including: Pulsating variable stars in clusters, RR Lyrae stars in globular clusters, and Cepheid variables in open clusters, i.e., in populations of known ages and metallicities (see Hambleton et al. 2022 for a further discussion).

2.5.1. Clusters in the Galactic Bulge and Plane

The Galactic bulge and plane host roughly 2/3 of the Galaxy’s globular clusters, yet are burdened by the perennial problems of high extinction and extreme crowding. However, the cluster population is innately quite interesting; this region hosts some of the most metal-poor and metal-rich of the Galaxy’s clusters, as well as two massive clusters that are unlike any others known, hosting complex populations exhibiting multiple peaks in $[Fe/H]$ as well as evidence of distinct bursts of star formation separated by many Gyr. Terzan 5 (Ferraro et al. 2009; Origlia et al. 2011) has 3 metallicity peaks ranging from -1 to $+0.5$ dex; Liller 1 (Ferraro et al. 2021) has multiple age bursts including 12 and 1 Gyr.

The Blanco DECam Bulge Survey (Johnson et al. 2020; Rich et al. 2020) has shown how multicolor photometry, combined with Gaia astrometry along with application of the vector point plot to clean the globular cluster color–magnitude diagrams yields dramatically improved results. LSST will cover all of the bulge clusters with multicolor photometry, dramatically better image quality, and Gaia matching. This

trifecta of multicolor imaging, astrometry, and radial star counts to confirm cluster membership has already paid off. While new imaging technology such as the Variables in the Via Lactea (VVV) survey have uncovered many new candidate globular clusters in the bulge and plane, applying multicolor photometry and astrometry has shown some of these clusters are not real (Rich et al. 2020). Combining u -band photometry from the Blanco DECam Bulge Survey with Gaia astrometry has led to clear detection of multiple populations in bulge globular clusters (Kader et al. 2022) again emphasizing the value of deep u -band observations and multicolor imaging that LSST will offer.

The combination of outstanding multiband photometry with Gaia astrometry, as well as imaging in the infrared, will produce data of remarkable quality. Proper motion vector point diagrams can be used to clearly separate cluster stars from field members; additional Gaia data releases will only lead to dramatically improved results.

LSST will have some significant advantages in the bulge and plane. The uniformity of photometry, potential development of tools that provide high resolution dereddening of the data by taking advantage of the multicolor photometry will be of great use in studying the clusters and their field populations. The multicolor data will yield robust metallicity and (for those clusters with sufficiently deep photometry) age estimates. If imaging can span multiple epochs, new variable star populations will be uncovered as well.

In order to exploit fully the promise of LSST, the astrometric solution of Gaia will need to be extended to faint magnitudes, so that eventually photometric cleaning may be applied to stars fainter than the Gaia limit of $g \sim 21$. If excellent astrometry is achieved to $g = 24$ or fainter, we gain leverage on many other important problems, such as the search for ultra-faint dwarf galaxies

2.5.2. Multiple Stellar Populations

Over the past two decades the presence of Multiple Stellar Populations (MSPs) in Galactic Globular Clusters has been well established as the norm (see Bastian & Lardo 2018 and Gratton et al. 2019 for recent reviews on the topic). In essentially all well studied GCs at least two populations have been identified: one that has similar abundance patterns to surrounding halo stars and a second population that tends to be enriched in Helium and, more importantly, presents negative correlations between some light elements (e.g., C, N, Na, O). Spectroscopic studies have provided an in-depth picture of these chemical differences; however, such studies are limited to a small fraction of GC stars (Carretta et al. 2009). Meanwhile, many groups have been successful in using space- and ground-based photometric observations to separate and characterize the populations in a large number of clusters (Lardo et al. 2011; Piotto et al. 2015; Hartmann et al. 2022; Leitinger et al. 2023).

However, so far wide-field studies of MSPs only encompass a limited number of clusters.

The LSST project has a great potential to expand this field. The majority of spectral features that can be used to differentiate between populations in GCs are concentrated in the bluer parts of the spectrum and the SDSS u -band is a valuable tool for distinguishing them. Because the majority of the Galactic GCs will be inside the footprint of LSST, a homogeneous analysis of a large set of clusters will be possible. The expected depth of the multi-epoch survey (well below the turn-off in most clusters) will also allow for a view of MSPs from the main sequence to the red giant and asymptotic giant branches. The wide field nature of the survey will be important in understanding how the populations behave far away from the cluster center and synergies with Gaia can help expand our understanding of the dynamics of the different stellar populations (see e.g., Martens et al. 2023).

3. Semi-resolved Star Clusters in the Local Group

By “semi-resolved star clusters,” we mean objects similar to the star clusters in the MCs. Such clusters can be fully resolved into stars only through diffraction-limited imaging with space telescopes like HST, or adaptive-optics-assisted imaging from the ground. On the other hand, imaging with $\sim 1''$ resolution from the ground already allows detailed studies of the brightest stars and the variables, as well as integrated photometry. Therefore, such clusters lie in a transition region between “resolved stars” and “integrated light only.” The advantage of LSST in regard to these clusters is that, for the first time, the same survey (and same filters) will cover huge numbers of clusters over the entire resolution scale going from resolved MW clusters to unresolved star clusters beyond the Local Group. This study will be even more powerful when combined with Euclid (Guy et al. 2022).

With the expected resolution of Rubin (median seeing of $\sim 1''$, best seeing of $\sim 0''.7$), we expect to measure the photometry of the brighter stars in semi-resolved clusters, especially in the cluster outskirts.

Single epoch observations with LSST will be deeper ($r = 24.5$) than most existing surveys of the MCs (STEP, SMASH) and will reach the main sequence turnoff at old ages if the effects of crowding are ignored. Given the large number of epochs with LSST, the best images will have significantly better seeing ($\sim 0''.7$) than these surveys ($\sim 1''.1$).

We can better appreciate the likely role of Rubin by examining the observational situation of the very populous clusters in the MCs. A hundred of them have HST photometry in at least 2 filters (e.g., Milone et al. 2022), and can be regarded as references for the definition of an age and metallicity sequence for MC stellar populations. Since the HST resolution is unbeatable (but for JWST), these clusters can be used to test the LSST photometry pipeline, as well as the

analysis tools, results and data products. For clusters without HST imaging, the targeted adaptive optics imaging survey VISCACHA (Maia et al. 2019; Dias et al. 2020) provides a first idea of the improvements that will be possible with LSST. VISCACHA reaches a similar depth to a single LSST epoch but with better image quality ($\sim 0''.5$), with available data for more than 230 clusters in the outskirts of LMC, SMC and Magellanic Bridge. On the other hand, Rubin will provide imaging in six bands, which is better for constraining metallicity and reddening.

Moreover, LSST will significantly improve the time-series data, providing the most extensive survey of variable stars in the MCs since OGLE IV (Udalski et al. 2015).

3.1. Census and Properties of Star Clusters in the Magellanic Clouds

The star cluster system of the MCs has always been one of the most studied for the following reasons: (i) they are sufficiently close to allow us to resolve their individual stars from the ground; (ii) a significant number of star clusters are sufficiently massive to populate the evolutionary phases following the Turn-Off; (iii) the SCs in the Magellanic system are present in great numbers. Indeed, the updated catalogs by Bica et al. (2008, 2020) include more than 4000 objects, comprising star clusters and young associations. A significant sub-sample of MC star clusters is also as populous as the old GCs of the MW, but with the difference that they span a wide range of ages, from a few Myr to 10 Gyr, making them suitable to probe a broad parameter space and to study how their physical and structural properties evolve during their lifetime. Furthermore, the Magellanic Clouds have massive young and intermediate age clusters that are not seen in the Milky Way. Additionally, since we observe the Clouds from outside of the galaxies and due to their lower metallicity, the extinction effects are significantly less than for much of the Milky Way.

In this context, the LSST survey will provide us with unprecedented data with respect to what is currently present in the literature. The major advantage will be the availability of deep, precise and homogeneous photometry in six bands. This unique data set will allow us to achieve the following goals:

1. *Completion of star clusters census in the MCs system.* It has been suggested (see e.g., Gatto et al. 2020, and references therein) that a conspicuous number of star clusters is still missing, especially in the LMC. This is due to several factors: (i) the too-shallow photometry used to search for star clusters in certain regions of the MCs, which hampered the ability to detect low-mass faint star clusters and biased the detection toward young and intermediate-age star clusters compared with the old ones of similar mass (ages larger than ~ 5 – 7 Gyr) which are fainter; (ii) crowding in the bar of the LMC and the main body of the SMC, resulting again in biasing the detection

toward more massive star clusters; (iii) inhomogeneous photometry in different regions.

It is difficult to estimate the number of new star clusters which will be detected based on the LSST deep photometry, however, Figure 19 by Gatto et al. (2020) seems to suggest that several hundred star clusters are still missing in the LMC only, especially in the Bar and at galactocentric radii >3 deg (a point where the coverage of the available wide-field surveys starts to be incomplete and more in-homogeneous).

2. *Measurement of the star cluster parameters (age, distance, metallicity, reddening).* The deep LSST photometry will allow us to reach some magnitudes below the turn-off magnitude of the oldest MC star clusters. This means that we can exploit their CMDs to accurately estimate the age, distance, metallicity and reddening of almost all the star clusters in the MCs, after a proper decontamination of field stars. It will also be possible to investigate the luminosity and mass functions of the clusters down to very low stellar masses. For the most crowded clusters, we will take advantage of the single images obtained during the best-seeing conditions, which will be deep enough to reach at least two magnitudes below the turn-off of the oldest cluster. The use of six bands in the procedure will allow us to some extent to remove the degeneracy between age, reddening and metallicity. The integrated photometry of MC star clusters can be directly compared to those of star clusters in more distant galaxies.
3. *Determination of star cluster structural parameters:* The LSST data will allow us to build accurate surface brightness profiles (SBPs) which contain information about the internal structure of the clusters. In particular, for each cluster, by fitting the SBP with Elson or King profiles (King 1962; Elson et al. 1989; Elson 1991) it will be possible to measure the core (and tidal) radius, the peak SB and the total luminosity. In turn, these data can be used to estimate the mass of the cluster by means of, e.g., Monte Carlo experiments on synthetic CMDs.

In turn, the measurements described above will allow us to explore the following issues, some of which represent long-standing open problems:

1. *Age gap puzzle of the star clusters in the LMC.* The existence of the so-called “age-gap,” an interval ranging from 4 to 10 Gyr in the LMC, which was thought to be almost totally devoid of star clusters (e.g., Da Costa 1991) has puzzled researchers for decades now. However, recent investigations based on relatively deep photometry have shown that several faint candidate star clusters in regions of the LMC not investigated before can have ages falling in the age-gap (Gatto et al. 2020). In addition, a re-analysis of the CMDs of the star clusters KMHK 1592 and KMHK 1762 based on deep photometry showed that both star clusters fall inside the age-gap, at odds with previous age estimates based on too-shallow photometry (Gatto et al. 2022; Piatti 2022). These findings seem to suggest that the age-gap is not a real physical feature, but the result of an observational bias, originated by the combination of too-shallow photometry carried out in the literature, the lack of a proper decontamination of field stars and an incomplete investigation of the LMC outskirts, where the lower stellar density of the field permits the detection of even faint and sparse star clusters.
- In this context, the contribution of the LSST survey will be to resolve any remaining doubt about the age-gap explanation, as it will allow obtaining both a complete census of the star clusters in the LMC outskirts, with the possible detection of old and faint star clusters not detected before, and to obtain CMDs deep enough to revise the ages of thousands of star clusters whose ages can in principle be very inaccurate, due to the shallowness of the photometry.
2. *Star Formation History of star cluster systems and comparison with the field.* The completeness of the star cluster census and the accuracy of age and metallicity estimates that will be possible with the LSST data will allow us to put significant constraints on the star cluster formation history and to compare it with the field star formation history. In this way, it will be possible to test one of the paradigms of star formation, which forecasts that a significant fraction of stars is formed within star clusters (Lada & Lada 2003). At the same time, the comparison between the star cluster formation histories of the LMC and SMC could allow us to verify whether the star cluster formation history has been triggered by multiple close encounters between the two MCs (and possibly between the MCs and MW), as recently suggested for the field stars (Massana et al. 2022), as well as to verify epochs of variation in the age–metallicity pattern followed by increases in the star formation rate, in order to understand the complex history of the system.
 3. *Star clusters 3D geometry, radial gradients.* The individual homogeneous estimates of metallicity, distance and reddening for the whole sample of star clusters in the MCs will allow studying of the tridimensional geometric distribution of the star cluster systems and compare it with that obtained from other tracers, such as the RC stars, as well as Cepheids and RR Lyrae variables. It will be possible to investigate possible gradients of age or metallicity coupled with radial migration or the interaction history of the MCs (e.g., Dias et al. 2016). Moreover, for clusters with precise radial velocity measurements, the proper motion given by the LSST multi-epoch data will provide a complete 6D space-phase vector (coordinates,

distance, proper motions and radial velocities). This can lead to strong conclusions, regarding expanding or stretching structures in the MCs outskirts (which can be compared to dynamical models; e.g., Dias et al. 2022), as well as possibly clusters with different velocity distributions than of the host galaxy.

4. *Physical processes governing the MC star clusters internal structure.* It will be possible to explore the evolution of the ensemble SC's structural parameters mass and radii with age and position in the galaxies. In particular, it will be possible to investigate the dynamical status of each star cluster and e.g., individuate the physical mechanisms that induce the observed increase of the core radius after 0.3–1.0 Gyr (e.g., Mackey & Gilmore 2003; Gatto et al. 2021). The data available for thousands of star clusters will allow us to study the mass-size relationship almost over the entire range of encompassed by the star clusters in the MCs, from hundreds up to hundreds of thousands of solar masses.

3.2. MC Clusters Contribution to Studies of Stellar Evolution

MC clusters have been very important in the stellar evolution theory because of the presence of very populous clusters of young and intermediate ages, unlike the old classical globular clusters of the MW and the generally low mass Galactic population of young clusters. Some of the MC clusters contain impressive numbers of evolved stars, such as for instance NGC 1866 with its 24 Cepheids (Welch & Stetson 1993; Musella et al. 2006), and NGC 419 with its ~ 20 carbon stars (Frogel et al. 1990). Even the most populous clusters in the MW and in M31 do not host more than one example of such objects (see e.g., Senchyna et al. 2015; Girardi et al. 2020; Marigo et al. 2022; Riess et al. 2022). The most populous MC clusters have been target of HST proposals, revealing surprising features such as broad MSTOs (Mackey et al. 2008; Milone et al. 2009), split main sequences (Milone et al. 2016; Correnti et al. 2017), dual red clumps (Girardi et al. 2009) and UV-dim MSTO stars (Milone et al. 2022), nowadays attributed mainly to the presence of a large fraction of fast rotators among the early-type stars of these clusters (e.g., Kamann et al. 2020, 2023; Martocchia et al. 2023). Although LSST photometry cannot compete with HST photometry for the densest clusters, it will cover the entire LMC and SMC areas with extreme homogeneity, multiple filters and long time series, hence making it possible to:

1. Improve the correction of their foreground extinction, and the contamination from the LMC and SMC fields. Indeed, this is a weak point of HST photometry, for which the observations are often available in only 2 filters and covering too small areas to allow proper decontamination
2. Look for the signatures of fast rotation (broad turn-offs, split main sequences, UV-dim stars) in sizeable samples of clusters including less populous objects, then allowing to explore open questions like: Are fast rotators more frequent in the most massive clusters than in small clusters and in the general galaxy field? Are slow and fast rotators truly coeval, and hence a single stellar population (e.g., Correnti et al. 2021)? Does the stellar rotation occur with a preferential orientation inherited from the molecular cloud from which the star cluster was formed (e.g., Kamann et al. 2019)? What is the role of close binary evolution (e.g., Wang et al. 2020; Kamann et al. 2021)?
3. Increase the numbers of variables in MC clusters, possibly adding constraints to the evolution of convective cores. For instance, fast rotation gives origin to larger H-exhausted cores at the end of the main sequence, hence causing a spread in the mass–luminosity relation of evolved stars. This spread could be documented in a number of ways, in particular (1) using the mass–radius relation derived from double-line eclipsing binaries, whenever one of the components is already evolved away from the zero-age main sequence; and (2) using mass estimates from Cepheids (Marconi et al. 2013; Costa et al. 2019).

3.3. Beyond the Magellanic Clouds

Besides star clusters in the Magellanic Clouds, LSST will image star clusters in other Local Group galaxies. At larger distances crowding will present even more substantial challenges than it does in the Magellanic Clouds, limiting our ability to study these star clusters using their resolved color–magnitude diagrams. Even if LSST only provides photometry of the brightest giants in the cluster outskirts, imaging with Rubin will still allow the structural parameters as well as the integrated photometry to be measured (see Huxor et al. 2014; Mackey et al. 2019 for a demonstration of ground based cluster studies in the Local Group).

A number of Local Group dwarf galaxies are known to host star cluster systems. Within the LSST survey footprint, the Fornax dSph hosts a surprising number of GCs—6—for its stellar mass (Pace et al. 2021), the dwarf irregular galaxy NGC 6822 hosts eight old GCs (Veljanoski et al. 2015) and a population of younger clusters (Chandar et al. 2000; Krienke & Hodge 2004). On the outskirts of the Local Group the WLM dIrr shows a single old GC (Hodge et al. 1999). In addition, the Eridanus II dSph hosts a single low mass star cluster (Koposov

et al. 2015; Crnojević et al. 2016) and the dIrr IC 1613 hosts a small number of low mass star clusters (Wyder et al. 2000).

Besides providing homogeneous measurements of known star clusters, LSST will allow for a systematic search for star clusters in Local Group dwarf galaxies. Together with star clusters in the Milky Way and the Magellanic Clouds, these cluster populations can be directly compared with those in more distant galaxies (see next section).

4. Extragalactic Star Clusters

4.1. Motivation

Beyond the Local Group, star clusters cannot be resolved into their constituent stars and must be studied using their integrated light. There is a wealth of previous imaging studies of star clusters young and old from the ground and from space. Surveys such as the SLUGGS survey (Brodie et al. 2014) of massive early-type galaxies and their globular cluster systems and the LEGUS survey of star-forming galaxies (Calzetti et al. 2015) have targeted representative samples of galaxies. Our understanding of old globular clusters is dominated by studies of Local Group galaxies and early-type galaxies in the Virgo and Fornax clusters (Côté et al. 2004; Jordán et al. 2007a). Large studies of young star clusters with HST such as LEGUS (Calzetti et al. 2015) and PHANGS-HST (Lee et al. 2022) do provide representative but not volume-limited samples of star-forming galaxies in the local universe. Much of the work on globular clusters has focused on massive early-type galaxies since they have populous GC systems and their relatively simple morphologies and light distributions make studying their star cluster populations easier. Work on other galaxy types has been fragmented and heterogeneous, often galaxy-by-galaxy, making comparisons difficult.

Most imaging studies have utilized imagers with fields-of-view smaller than the full extent of the star cluster systems, and this is particularly acute for studies with HST. At the distance of the Virgo Cluster (16.5 Mpc, Mei et al. 2007), a single HST ACS pointing covers 16 by 16 kpc. While this field of view can comfortably contain the GC system of a dwarf galaxy, the globular cluster systems of more massive galaxies extend beyond 100 kpc (AM-1 is 120 kpc from the center of the MW; Dotter et al. 2008; PAndAS-48 lies 160 kpc in projection from M31; Huxor et al. 2014) thus carrying out an accurate census of the GC systems of luminous ellipticals requires imaging that covers a radial distance of >120 kpc from the galaxy center; Dirsch et al. 2003; Rhode & Zepf 2004). Only the widest-field ground based imagers (e.g., MegaCAM on CFHT, the twin MegaCAM at Magellan, OmegaCam on VST, Hyper Suprime-Cam on Subaru, the Dark Energy Camera on CTIO, the One Degree Imager on WIYN) can image the entire GC system of a massive galaxy in a single pointing. Ideally, one wants the imaging to extend beyond the GC system in order to (for example) accurately quantify the radial extent of the GC

system, determine the extent of intragroup/cluster GCs (see e.g., Chies-Santos et al. 2022) and to more easily estimate the level of contamination from foreground or background objects in the GC candidate sample. Due to its wide field nature, LSST will allow entire GC systems to be imaged. Furthermore, selection of GC candidates via photometry in six filters will yield cleaner GC candidate samples and while its high image quality will help eliminate non-GC extended sources such as background galaxies with similar colors. The wide wavelength coverage provided by LSST will also allow the physical properties of extragalactic star clusters to be better constrained.

LSST presents the first opportunity to perform a large scale, homogeneous census for extragalactic globular clusters, as well as identifying intergalactic globular clusters and hypervelocity clusters (e.g., Caldwell et al. 2014). We briefly discuss some of the impacts Rubin will have on our understanding of extragalactic star cluster systems including young star clusters, globular clusters and nuclear star clusters before discussing in more detail the science that will be enabled by the discovery of massive numbers of star clusters.

4.1.1. Extragalactic Nuclear Star Clusters

Nuclear star clusters (NSCs) are dense star clusters at the centers of galaxies have masses ranging from 10^5 to $10^7 M_{\odot}$ and effective radii of only a few parsecs (Stone et al. 2017; Neumayer et al. 2020). Studies such as Baldassare et al. (2022) have searched for massive black holes at the centers of nuclear star clusters, and the larger sample identified by Rubin will be able to extend these studies as well as provide full band photometric constraints on the nature of the star clusters. Sánchez-Janssen et al. (2019) studied NSCs in Virgo Cluster galaxies, finding a close connection between properties of NSCs and globular cluster systems (GCSs) of low mass galaxies. Zanatta et al. (2021) found a high occurrence of nuclear star clusters in faint Coma galaxies and that the mass of the host galaxy is the major driver of the efficiency of NSC formation and that the environment plays a secondary role. Carlsten et al. (2022) studied NSCs in the satellites of Milky Way-like galaxies in the Local Volume, finding lower nucleation fractions than for cluster galaxies, but similar connections between NSCs and GCSs. Rubin studies will extend these studies to larger samples of galaxies over a greater range of environments and morphological types, providing additional constraints on formation models.

4.1.2. Extragalactic Young Massive Clusters

A significant fraction of stars forms in bound stellar clusters hence understanding clustered star formation is important for understanding star formation in galaxies. Studies of the most massive young star clusters in the local universe can inform our understanding of how globular clusters formed. Since the stars in a cluster are concentrated

both spatially and temporally, the feedback from star clusters is likely more efficient than low density star formation. Depending on how the stellar initial mass function is sampled, the most massive stars may only be found in young star clusters.

Young star clusters are typically found in star-forming galaxies, which are morphologically complex. Due to this complexity, studying young star clusters in star-forming disks typically requires space based imaging. The angular resolution of Rubin is $\sim 1''$, a factor of ten larger than the angular resolution of HST. For nearby galaxies (within ~ 10 Mpc), Rubin observations have similar spatial resolution to those of more distant galaxies observed with HST, for example the Hubble imaging Probe of Extreme Environments and Clusters (HiPEEC) survey of six merging galaxies (Adamo et al. 2020). The Rubin observations are likely limited to the fainter outskirts of galaxies and the brightest star clusters (i.e., the youngest and most massive). The larger sample of galaxies provided by LSST will provide context to more detailed studies with HST and JWST (e.g., A. Adamo et al. 2023, in preparation; Whitmore et al. 2023).

Active areas of research in young star clusters include how the initial cluster mass function varies between and within galaxies (e.g., Larsen 2009; Wainer et al. 2022) and how the fraction of stars formed in bound clusters varies (e.g., Larsen & Richtler 2000; Goddard et al. 2010; Silva-Villa & Larsen 2011; Adamo et al. 2015, 2020; Chandar et al. 2017). Additionally, studies of the spatial correlations between young star clusters, molecular clouds and H II regions allow the timescales of each of these stars of star formation to be constrained (Kruijssen et al. 2018; Peltonen et al. 2023).

Rubin studies of young star clusters will target the physics of star cluster formation, and the u -band photometry will be key to breaking the age-extinction degeneracy. In particular, the data will be able to target the following questions:

1. How does the truncation mass of the initial cluster mass function vary with galaxy properties?
2. How do the properties of nearby young star clusters compare with those of star-forming clumps observed in high-redshift lensed galaxies (e.g., Mowla et al. 2022; Claeysens et al. 2023)?
3. What are the evolutionary links between young star clusters and older globular clusters?

4.1.3. Extragalactic Globular Clusters

Well-characterized extragalactic clusters can be used to extend our knowledge of galaxy structure, and the Rubin observations of extragalactic globular clusters will be able to measure ages, masses and metallicities from integrated light, probing different environments and galaxy ages. A further discussion of this takes place in Section 4.2.3.

4.1.4. Science Cases

The dark matter content of galaxies: Globular clusters provide a number of probes of the dark matter content of galaxies, including the globular cluster-halo mass scaling relation, the timing problem in dwarf galaxies, as tracers of the galaxy potential and as tracers of the dark matter surface density, as is described in the next paragraph.

Recent literature has claimed that there is a one-to-one relationship between mass in globular clusters and galaxy halo mass over a wide range of halo masses (Blakeslee et al. 1997; Spitler & Forbes 2009; Hudson et al. 2014; Forbes et al. 2018; Zaritsky 2022). These results imply that counting the size of a galaxy’s GC population would be an observationally inexpensive way to measure its halo mass. While there is strong evidence for the one-to-one relation in massive galaxies (e.g., Forbes et al. 2016), there are theoretical reasons (Choksi & Gnedin 2019; El-Badry et al. 2019; Bastian et al. 2020) to expect that the relation breaks down in low mass galaxies. In fact, in spite of some Local Group dwarf galaxies containing relatively high numbers of GC for their masses (see Section 3.3), there must be a breakdown at some point, since most of the lowest-mass galaxies do not host globular clusters (e.g., Eadie et al. 2022). The globular cluster mass-galaxy halo mass relation shows increased scatter at low galaxy masses (Forbes et al. 2018) so again, constraining it with larger numbers of galaxies will be beneficial.

It was first noted by Tremaine (1976) that the half-dozen globular clusters in the Local Group Fornax dSph have ages much greater than their calculated orbital decay times. Dwarf galaxies are presumed to be dark matter dominated. If their central dark matter profiles are cuspy, as predicted by collisionless cold dark matter only simulations, one or more of the GCs in Fornax dSph should have inspiralled to the center due to dynamical friction. If their central dark matter profiles are cored, either due to baryon feedback or more exotic dark matter physics, the effects of dynamical friction are weaker, and less inspiralling would occur. Globular cluster systems of these galaxies thus place important constraints on the nature of dark matter (Bar et al. 2021). An issue with such studies is that any given galaxy has only a small number of clusters. One way around this is to “stack” cluster systems as in Sánchez-Salcedo & Lora (2022), and hence the larger number of galaxies observed by Rubin will be of enormous benefit.

There is a long history of using GCs as test particles in larger galaxies’ halos. Spectroscopy is required to obtain radial velocities for mass modeling, generally preceded by imaging to identify target GCs and to quantify their spatial distribution. Simulations show that good kinematic information of at least 150 GCs per galaxy is required to recover the mass and radial distribution of the DM halo using dynamical models in extragalactic systems (Hughes et al. 2021). Nonetheless, we can use the projected number counts of GC populations

obtained with Rubin/LSST, alongside their galaxy stellar masses, to trace the structure of their host DM haloes, which is much less observationally demanding than observing the faint and diffuse stellar halo in the galactic outskirts (Reina-Campos et al. 2021).

Low surface brightness science: Star clusters can make significant contributions to our understanding of the low surface brightness universe. Intragroup and intracluster GCs (e.g., Taylor et al. 2017; Harris et al. 2020) can be used to probe kinematics of large-scale dark matter halos and trace galaxy assembly history. They can be used for similar purposes on smaller spatial scales where found associated with stellar streams and shells in individual galaxy haloes (e.g., Veljanoski et al. 2014; Kang et al. 2022). Star clusters in ultra-diffuse galaxies (UDGs) have recently received significant attention as both signposts to find UDGs and as indicators of UDG origins (e.g., Li et al. 2022; Jones et al. 2023) Rubin/LSST will provide a large sample of UDGs as well as “normal” dwarf galaxies allowing comparison between the GC populations of different types of dwarf galaxies.

Star cluster formation: There are two broad models for the origin of GCs. Motivated by the old GCs of the MW and the lack of GC mass star clusters forming today in the MW the older model (e.g., Peebles 1984; Trenti et al. 2015) of GC formation requires special conditions in the early Universe. In the more modern model (e.g., Elmegreen & Efremov 1997; Elmegreen 2010; Kruijssen 2015), motivated by observations of young star clusters with similar or higher masses to GCs in local starburst galaxies (e.g., Whitmore & Schweizer 1995; Holtzman et al. 1996; Adamo et al. 2020), all star cluster formation shares a common process. These two models make very different predictions about the age distribution of GCs. In the older model all GCs should have similar old ages while in the modern model, the age distribution varies galaxy-to-galaxy depending on the formation history; since a high star formation rate density is required to form $>10^5 M_{\odot}$ of stars within a few parsecs in a few Myr, massive star clusters trace periods of high star formation. Evidence for this modern model has emerged via observations of younger GCs in lower mass galaxies (e.g., Chandar et al. 2006; Sharina et al. 2006; Mora et al. 2008; Parisi et al. 2014; Fahrion et al. 2020) and from studies that find a connection between assembly history of galaxies and the ages and metallicities of their GCs (e.g., Forbes & Bridges 2010; Usher et al. 2019b; Kruijssen et al. 2020).

Simulations (e.g., Li & Gnedin 2014; Pfeffer et al. 2018; Valenzuela et al. 2021; Rodriguez et al. 2023) based on these models make quantitative predictions that can be tested with observation from LSST. The volume limited sample of GC systems provided by Rubin will be easier to compare with simulations than existing targeted studies. Observations of young star clusters will be used to constrain models of star cluster formation.

Galaxy formation: Assuming that GCs are the natural outcome of intense star formation, the properties of GCs can be used to study the formation and assembly history of their host galaxies. The ages of GCs directly indicate when intense star formation occurred. By inverting the redshift dependent galaxy mass–metallicity relation, the metallicity and age of a GC can be used to infer the likely mass of the galaxy it formed in Kruijssen et al. (2019). Measurements from multiple GCs can be combined together to study the mass assembly history of a galaxy. Since more massive and earlier mergers deliver their GCs on tighter orbits (Pfeffer et al. 2020), by combining the ages, metallicities and orbits of GCs the assembly history of a galaxy can be reconstructed in detail as was done by Kruijssen et al. (2020) for the MW.

Even when limited more information is available, Kruijssen et al. (2019) showed that correlations exist between global GC properties like the number of GCs, the mean age and the slope of the age–metallicity relationship and the assembly history of a galaxy at fixed stellar mass. LSST will provide a huge number of galaxies with well characterized GC systems. Assembly histories derived from these GC systems can be compared to the predictions of simulation of galaxy formation. LSST will also act as the input catalog and provide context to spectroscopic studies that would enable more detailed assembly history studies.

Globular cluster systems as distance indicators: The GC luminosity function has long been promoted as a distance indicator, with systematic uncertainties at the 0.3 mag level (Villegas et al. 2010; Rejkuba 2012). GCs are also a systematic in surface brightness fluctuations, where they need to be masked lest they contribute extra power to the fluctuations (Jensen et al. 2015). Mean GC sizes have also been proposed as standard rulers (Masters et al. 2010). Although Rubin will only be able to measure reliable sizes for relatively nearby GCs, due to the nature of the survey, it will increase the numbers of cluster systems sampled which will naturally allow the details of this distribution to be further probed.

Stellar population variations in globular clusters across galaxies: Over the past two decades many works have demonstrated nonlinear color–metallicity and color–color relations in GC systems (e.g., Blakeslee et al. 2012; Chies-Santos et al. 2012; Lee et al. 2019; Fahrion et al. 2020). Usher et al. (2012, 2015) found that the relationship between GC color and metallicity varies between galaxies. Recently, it was found that the color–color relation of GCs in different regions of the Virgo cluster behaves differently, implying that cluster formation happens differently in different environments (Powalka et al. 2016). There is also evidence for variation in the age distribution of globular clusters between galaxies (Chies-Santos et al. 2011; Usher et al. 2019a, e.g.,). The range of galaxy environments and morphologies probed by these studies is incomplete: for example, they do not include clusters belonging to low surface brightness galaxies. The

homogeneous, ultra-deep multi-band imaging from LSST/Rubin will allow us to obtain a complete census of color–color relations up to $z = 0.05$ and investigate this in unprecedented detail. Synergies with Euclid and Roman will extend the baseline to redder colors, as detailed in Section 4.5.

High-Energy Astrophysics: Young star clusters, particularly the more massive ones, may also provide clues to the formation channels for mass gap black holes (e.g., Mapelli & Zampieri 2014; Rastello et al. 2020, 2021; Di Carlo et al. 2021). One of the best observational candidates for an intermediate mass black hole, ESO 243–49 HLX-1 (Farrell et al. 2009), may also be hosted by a young star cluster (Farrell et al. 2012). Rubin’s unprecedented survey will provide a comprehensive data set on clusters that will allow for multi-wavelength follow-up to provide further observational constraints on X-ray binary and intermediate mass black hole candidates in young massive star clusters (e.g., Rangelov et al. 2012).

Globular clusters are also intimately linked with high-energy astrophysical events: novae (Kato et al. 2013; Doyle et al. 2019), supernovae (Voss & Nelemans 2012; Washabaugh & Bregman 2013), fast radio bursts (Kirsten et al. 2022) and many X-ray binaries, including ultraluminous X-ray sources (ULXs) (Maccarone et al. 2007). The remnant population of globular clusters can shine light on understanding the progenitors of transients, including gravitational wave events (Dage et al. 2020; Athukoralalage et al. 2023). Due to their relatively simple stellar populations, it is easier to measure the age and metallicity of a star cluster than field starlight, allowing the progenitor of a transient to be constrained. Unlike the stellar progenitors of transients, star clusters will survive transients relatively unchanged, allowing the progenitor of past transients to be studied.

Many of the ULXs in globular clusters have been identified using archival HST and Chandra Observatory observations of galaxies in the Virgo and Fornax clusters (e.g., Dage et al. 2021). However, this method is observationally biased toward identifying clusters in the inner regions of the host galaxies; Hubble imaging cannot survey the entire cluster system of a massive galaxy. Chandra has a much larger field of view, and the practical outcome is that detected X-ray sources in the galaxy outskirts are often left unprobed due to lack of wide-field optical coverage.

X-ray population studies of extragalactic star clusters can also reveal the X-ray binary populations, allowing for a model of the X-ray luminosity functions of star clusters (Peacock et al. 2017; Lehmer et al. 2020; Hunt et al. 2023). These scaling relationships have further impacts on low-luminosity active galactic nucleus (AGN) identification, and feedback in AGN (Chadayammuri et al. 2022). Rubin’s more systematic and wide-field coverage will enable optical classification of the hosts of many of these sources and provide more spatially

complete surveys of the LMXB content of extragalactic cluster populations.

4.2. Tasks

4.2.1. Source Detection and Measurement

Before sources can be classified as star clusters, they must be detected and their properties (flux and structural parameters) measured. This process can be broken down into three regimes on the basis of background galaxy surface brightness and the morphological complexity. For the faintest background galaxy light, such as the outer halos of galaxies and the intracluster light of galaxy clusters, the output of the default LSST source detection and photometry pipeline will likely suffice. For brighter galaxies with relatively simple morphologies, i.e., early-type galaxies, the established approach is to subtract the galaxy light, either using a parametric model for the galaxy light or using a median filter image, perform the source detection step on the subtracted image then perform photometry on the original image. For more morphologically complex galaxies (i.e., star-forming galaxies), a more sophisticated deblending and source measurement process will be required. Best seeing stacks would be quite useful for size measurements and source detection in crowded fields. Understanding the completeness of source detection steps is critical, and comparison with HST and JWST imaging can be used to test source detection and measurement at higher spatial resolution. However, most extragalactic star cluster studies with HST have utilized shallower imaging than Rubin will provide, thus new approaches will be needed for characterization of faint star clusters.

4.2.2. Source Classification

Before star clusters can be studied they must be distinguished from foreground stars and background galaxies. Fortunately, the properties of star clusters are intermediate between those of stars and galaxies, making selecting star clusters a more general case of star–galaxy separation (e.g., Fadely et al. 2012; Slater et al. 2020). Old, massive star clusters have regular, round morphologies. Any objects with irregular or spiral morphologies, or that are highly elongated, can be classified as background galaxies. Only for the closest (~ 1 Mpc) star clusters, where their diameters are larger than the FWHM point-spread function (PSF), can individual stars be seen in their outskirts. In young low mass clusters, a handful of stars can dominate the light, giving a more irregular appearance. At least for star clusters within a few tens of megaparsecs, star clusters are less extended than a significant fraction of background galaxies with the same apparent magnitude. Thus relatively clean samples of star clusters can be selected by only using size and magnitude cuts (e.g., Jordán et al. 2009). Previous work (e.g., Harris 2009) has shown that

the effective diameter of a star cluster needs to be at least 10% of the PSF FWHM for the diameter to be effectively measured. For the median effective seeing of the survey ($1''.0$) and a typical GC with a radius 3 pc, this corresponds to a distance of 6 Mpc; for the best effective seeing expected ($0''.6$) this corresponds to a distance of 10 Mpc. Thus, LSST will only be able to effectively separate stars and star clusters on the basis of their sizes within a few Mpc (e.g., A. K. Hughes et al. 2021). However, even at larger distances, the high spatial resolution provided by Rubin will allow at least some of the background galaxy population to be separated from star clusters.

Since star clusters consist of stars with a range of temperatures, their position in color–color space is different than individual stars. Compared to a star with same color in the blue, say ($u - r$), a star cluster will have a redder color at longer wavelengths, say ($i - y$). Since star clusters formed their stars in a single burst and have evolved passively since, their position in color–color space is also different from actively star-forming galaxies, with star clusters being bluer at longer wavelengths than galaxies with the same colors at shorter wavelengths. Since the vast majority of star clusters that will be observed by Rubin are at redshift $z < 0.02$, the effects of redshift on the colors are minor compared to distant galaxies (Muñoz et al. 2014).

Finally, given that extragalactic star clusters are at distances of a megaparsec or more, their proper motions and parallaxes are insignificant, allowing anything with a non-zero proper motion or parallax to be selected as a star. Gaia astronomy can be used for the nearest and most massive star clusters (e.g., Voggel et al. 2020), with Rubin astrometry used later in the survey for fainter sources.

As a classification problem, selection of star clusters is well suited to machine learning techniques. Recent experiments with machine learning selection of clusters on either images (Pérez et al. 2021; Thilker et al. 2022) or photometric catalogs (Barbisan et al. 2022; Mohammadi et al. 2022) show promise. Samples of star clusters, foreground stars and background galaxies from space based imaging (HST or JWST) can be used to train and validate classification techniques with Rubin data; other efforts (photometric redshift pipelines from the LSST Galaxies collaboration, star–galaxy separation techniques from SMWLW collaboration) may also prove useful. Spectroscopically confirmed clusters provide another possible training set (radial velocity measurements clearly select between foreground stars, star clusters and background galaxies) but pre-targeted spectroscopy suffers from selection biases. Untargeted spectroscopy with integral field units (e.g., MUSE on the VLT) may prove useful to avoid such biases.

4.2.3. Star Cluster Property Inference

To learn about star clusters’ formation and evolution and that of their parent galaxy, their physical properties need to be

inferred. Masses, ages and metallicities of stellar populations can be measured by fitting stellar population models to observed photometry. Most imaging studies of GC systems have relied on imaging in two or three filters, often *gri* or their analogues, preventing the effects of age and metallicity from being disentangled. More filters and a wider wavelength coverage improve the constraints from fitting stellar population models, and the large number of filters provided by Rubin helps. As can be seen in the color–color plots in Figure 5, while strong degeneracies exist between age, metallicity and extinction for *gri*, the addition of *uzy* allows these degeneracies to be (partially) broken. Priors on extinction values can be obtained from far-infrared observations and/or SED-fitting the integrated light of the host galaxy, with a complication being the lack of a way to tell whether a given star cluster is in front of, embedded in, or behind its host galaxy. Spectroscopic observations will be useful for testing the ages and metallicities from Rubin photometry, with careful consideration of selection effects as noted above.

Multi-band photometry of extragalactic star clusters gives ages, metallicities, and relative masses. To measure the mass and physical extent of an extragalactic star cluster, its distance is required. Most star clusters are too close for reliable photometric redshifts (Muñoz et al. 2014), and in any case peculiar velocities comprise a large part of the observed redshift at the expected distances. The distance of an individual cluster is generally inferred from association with a host galaxy, which can be ambiguous if multiple galaxies are projected close together on the sky; for clusters in such locations, probabilistic galaxy membership better quantifies the limits of knowledge. With a measured distance and angular size, physical size can also be measured. Physical sizes of old star clusters are of interest to studies of their dynamical evolution; physical sizes of younger clusters also constrain the star formation process.

4.3. Deliverables

The ideal deliverables from a Rubin study of extragalactic star clusters include both a catalog of star clusters and a catalog of star cluster systems. The catalog of star clusters would include photometric and structural/size measurements; derived mass, age and metallicity; probabilistic classification (i.e., likelihood of being a star cluster; and probabilistic indication of parent galaxy). The catalog of star cluster *systems* would include estimate of population size, spatial distributions, mass functions, and age and metallicity distributions, taking into account the various selection effects of the Rubin observations.

4.4. Expected Extragalactic Star Cluster Sample

To allow classification of sources as star clusters and to allow some inference on their properties requires that sources be detected in multiple bands. For old stellar populations, typical of

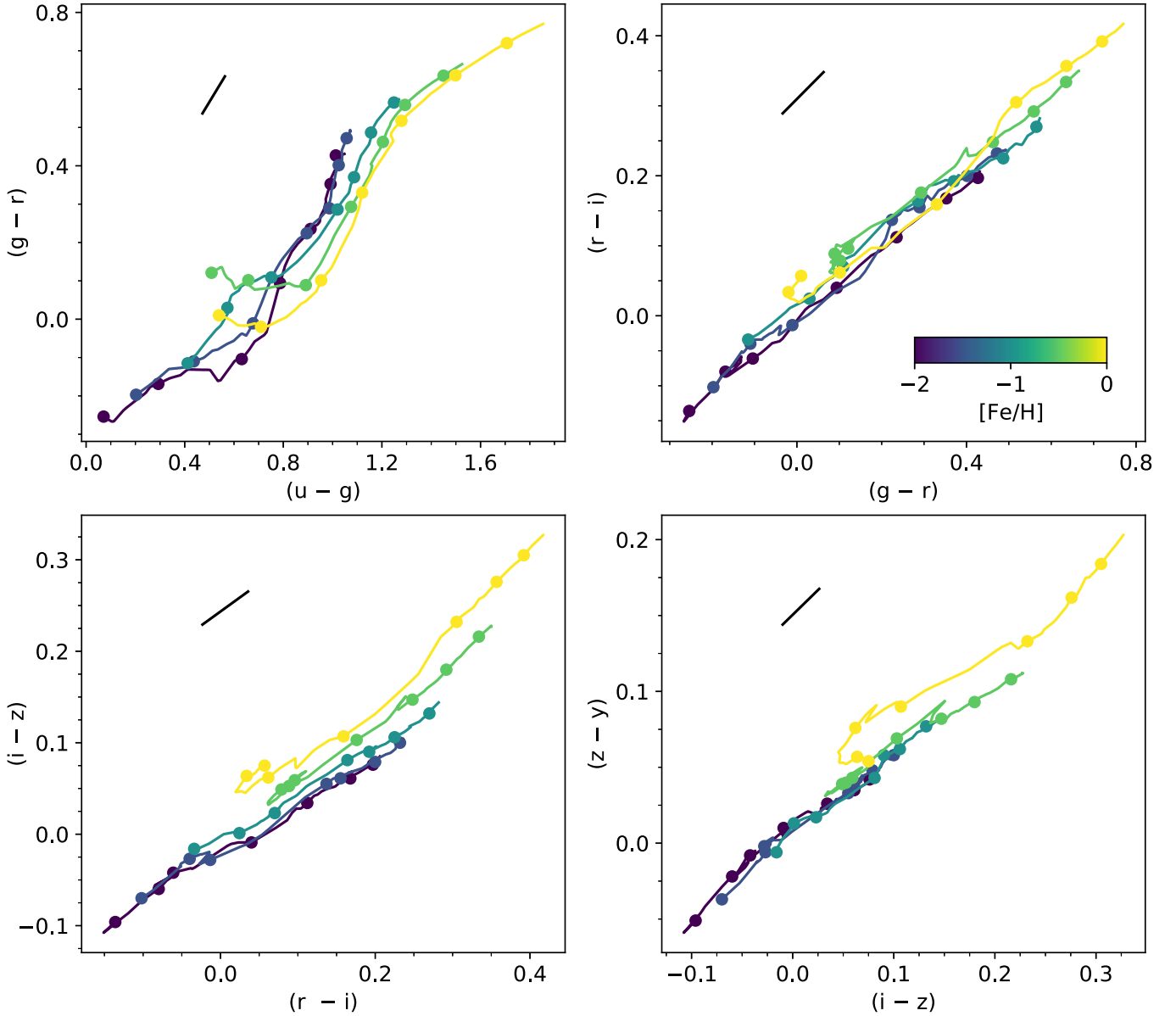


Figure 5. Color–color plots for model stellar populations in the Rubin bands calculated using FSPS (Conroy et al. 2009; Conroy & Gunn 2010). In each panel the lines show model tracks from 100 Myr to 14.1 Gyr for five metallicities color coded from $[\text{Fe}/\text{H}] = -2$ in dark purple to $[\text{Fe}/\text{H}] = 0$ in yellow. The circles show the models at 100 Myr, 200 Myr, 500 Myr, 1 Gyr, 2 Gyr, 5 Gyr and 10 Gyr. The black line corresponds to the reddening vector for $E(B - V) = 0.1$. Although strong degeneracies exist between age, metallicity and extinction for $(g - r)$ vs. $(r - i)$, the addition of u , z and y allows for these degeneracies to be broken.

most GCs (using the predictions of the FSPS models of Conroy et al. 2009; Conroy & Gunn 2010), and the expected depths of the final survey, a star cluster will first be detected in r and i , then in g and z , then in y and finally in u , with more metal-poor GCs being more easily detected in the blue and more metal-rich in the red. Since $(r - i)$ does not provide on its own a wide enough color baseline for effective selection or stellar population studies, we require detection in g to be the minimum required to study an old star cluster. For young (less than a few hundred million

years) star clusters, u -band photometry is important in disentangling the effects of age and extinction.

Based on the well-studied globular cluster luminosity function (GCLF, e.g., Jordán et al. 2007b) that peaks at $M_g \sim -7.5$, one can estimate that LSST will reach the turnover magnitude (TOM) of GC systems at 40 Mpc with single estimated exposures. For more nearby GC systems such as galaxies belonging to the Fornax Cluster, with one exposure, LSST will reach 1.5 mag fainter than the TOM of the GCLF

Table 1
Predictions for Extragalactic Star Clusters Observed with LSST

(a) Band	(b) m Visit	(c) m 10 yr	(d) N_{GC}	(e) M [Fe/H] = -2	(f) D	(g) M [Fe/H] = -1	(h) D	(i) M [Fe/H] = 0	(j) D	(k) M 100 Myr	(l) D
<i>u</i>	23.60	25.45	4×10^5	-6.40	24	-5.86	19	-4.56	11	-7.50	41
<i>g</i>	24.41	26.54	1×10^7	-7.44	64	-7.12	55	-6.36	39	-8.08	86
<i>r</i>	23.98	26.71	3×10^7	-7.86	82	-7.69	75	-7.11	58	-8.13	92
<i>i</i>	23.39	26.20	2×10^7	-8.07	72	-7.96	68	-7.51	56	-8.20	76
<i>z</i>	22.79	25.51	9×10^6	-8.15	53	-8.10	52	-7.83	46	-8.30	56
<i>y</i>	22.00	24.73	3×10^6	-8.19	38	-8.18	38	-8.03	35	-8.36	41

Note. (a) Rubin band. (b) Apparent magnitude median single visit depth for the WFD based on the `baseline_v3.0_10yrs` OpSim run (c) Apparent magnitude median coadd depth corrected for galactic extinction for the WFD footprint based on the `baseline_v3.0_10yrs` OpSim run. (d) Total number of GCs observed in the entire LSST footprint over 10 yr based on the `baseline_v3.0_10yrs` OpSim run. (e) absolute magnitude for a $2 \times 10^5 M_{\odot}$, 12.6 Gyr, [Fe/H] = -2 GC. (f) Maximum distance in Mpc GC a GC with absolute magnitude from (e) will be seen given the depth given in (c). (g) and (h) Same as (e) and (f) but for a [Fe/H] = -1 GC. (i) and (j) Same as (e) and (f) but for a [Fe/H] = 0 GC. (k) and (l) Same as (e) and (f) but for a $2 \times 10^4 M_{\odot}$, 100 Myr, [Fe/H] = 0 YMC.

with a single exposure. After 10 yr, we estimate that LSST will be able to reach the TOM of the GCLF of systems ~ 100 Mpc away and 1.5 mag brighter than the TOM for systems ~ 200 Mpc ($z \sim 0.05$). Thus, LSST will be able to provide a complete census of GC systems up to $z \sim 0.05$.

To estimate the number of GCs LSST will image, we combined the Eadie et al. (2022) relationship between galaxy stellar mass and mass in GCs with the Driver et al. (2022) galaxy stellar mass function. By assuming an average GC mass of $2 \times 10^5 M_{\odot}$, we calculated a GC volume density of 7.6 Mpc^{-3} . Using version 3.1 of the FSPS stellar population modeling code (Conroy et al. 2009; Conroy & Gunn 2010), we calculated the absolute magnitudes of a GC with a stellar mass of $2 \times 10^5 M_{\odot}$, an age of 12.6 Gyr (corresponding to a formation redshift of $z = 5$) and a metallicity of [Fe/H] = -1 in each of the Rubin bands which we give in Table 1. Assuming a Gaussian GC luminosity function centered on these magnitudes with dispersion of 1.2 mag (based on the MW’s V-band GC luminosity function from Harris 2001), by using the Healpix maps of coadded 5σ depth corrected for Galactic extinction from the `baseline_v3.0_10yrs` OpSim (Delgado et al. 2014) run, we can calculate the number of GCs across the sky LSST will likely detect over the course of the 10 year survey. These estimates are provided in Table 1. We also provide the median distances the model GC would be observed out to in the WFD footprint. These numbers are optimistic given that they do not account for the lower limiting magnitude due to the higher background caused by the host galaxy light, for the effects of crowding, or for any extinction internal to the host galaxy. We can use the same assumptions to estimate LSST will survey 100,000 galaxies each with at least 10 GCs detected in all of *griz*.

To account for the effects of metallicity we also calculated model photometry $2 \times 10^5 M_{\odot}$ 12.6 Gyr GCs with [Fe/H] = -2

and [Fe/H] = 0. The metal-poor GC is bluer and brighter while the metal-rich GC is redder and fainter although we note that measurements of the GC mass-to-light ratio in the MW and M31 (e.g., Strader et al. 2011; Dalglish et al. 2020) show a constant V-band mass-to-light ratio with metallicity. We provide the absolute magnitudes and median distance limits in Table 1.

The number of young star clusters LSST will observe is harder to estimate. The fraction of stellar mass that forms in bound clusters and the truncation mass of the initial cluster mass function depend on the star formation surface density, such that more rapidly forming regions form more mass in clusters and form more massive clusters.

In Table 1 we give absolute magnitudes and median distance limits for a $2 \times 10^5 M_{\odot}$ 100 Myr, [Fe/H] = 0 star cluster. We expect that detecting young clusters should suffer more from the effects of the host galaxy background, crowding and extinction than GCs since they are typically found in and around active star-forming regions. The case of the extreme starburst Haro 11 is instructive. Many of the young star clusters in this galaxy studied by Adamo et al. (2010) with HST are bright enough to be detected in a single LSST visit. However, given the spatial resolution of LSST, at a distance of 85 Mpc the star clusters blur together into a handful of star cluster complexes.

4.5. Synergies with Upcoming Missions

Rubin Observatory will have many synergies with upcoming and proposed missions. We highlight potential overlaps in star cluster science with a few of these.

Upcoming space-based wide field imaging missions like Euclid and the Roman Space Telescope will provide high resolution imaging and near-infrared photometry. The overlap between the Euclid Wide Survey and the extragalactic LSST WFD is about 9000 square degrees, or about half the LSST

WFD and 60% of the Euclid survey. Rubin and Euclid have many synergies, specifically by using joint pixel deblended photometry on peripheral regions of Milky Way globular clusters, as well as dwarf satellites and nearby galaxies. Combining the two surveys will also allow for a volume-limited survey of globular cluster candidates (Guy et al. 2022). About 4 million GCs will be detected at the 5σ level in both the Euclid VIS band and in the LSST *ri* bands and about 800,000 GCs will be detected in all the Euclid bands as well as the *grizy* LSST bands. About a quarter of the GCs detected in all four Euclid bands will be detected in *u*-band by LSST. Near infrared photometry would provide better star-globular cluster-galaxy separation (e.g., Muñoz et al. 2014; Cantiello et al. 2018) and provide stronger constraints on metallicity (e.g., Kissler-Patig et al. 2002; Cantiello & Blakeslee 2007; Chies-Santos et al. 2012) and even age (e.g., Chies-Santos et al. 2011; Georgiev et al. 2012; Tudorica et al. 2015). High spatial resolution imaging from space would allow star, globular cluster, and galaxy separation out to much greater distances using angular sizes.

The Nancy Grace Roman Telescope’s high precision astrometry and wide-field of view will enable studies of the entire tidal radius of a globular cluster,²⁵ as well as studies of multiple stellar populations in globular clusters and stellar kinematics of the cluster (Bellini et al. 2019). The field-of-view Roman’s Wide Field Instrument is also well matched to the size of GC systems nearby galaxies (140 by 70 kpc at a distance of 10 Mpc) allowing for high resolution near-infrared imaging of a galaxies GC system in a single pointing. Roman’s High Latitude Wide Area Survey will likely provide deeper (25.8 to 26.7 AB, similar depths to LSST) NIR photometry than Euclid over a smaller area (~ 1700 square degrees https://roman.gsfc.nasa.gov/high_latitude_wide_area_survey.html).

Future planned and proposed UV and optical missions such as CASTOR (Cote et al. 2019), UVEX, STAR-X, CSST (e.g., Qu et al. 2023) and ULTRASAT²⁶ will provide valuable UV coverage to Rubin’s full optical coverage. In particular, UV photometry would yield improved constraints on age, metallicity and extinction.

4.6. Summary

The Rubin data set will be transformative for a broad range of star cluster science. Rubin observations will detect the lowest-mass stars in the nearest Milky Way clusters and the integrated light from the brightest clusters in galaxies at distances of 100 Mpc. With these data, questions of formation and evolution of stars, star clusters, and galaxies can all be addressed. This roadmap does not represent an exhaustive catalog of every topic that can be addressed with Rubin data:

²⁵ https://www.stsci.edu/files/live/sites/www/files/home/roman/_documents/roman-capabilities-stars.pdf









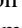
²⁶ <https://www.weizmann.ac.il/ultrasat/>

the buildup of galaxy haloes from dissolving star clusters and their relationship with stellar streams; and stellar variability in Galactic clusters are just a few examples of star cluster topics not mentioned above. The most exciting prospect is the new questions that will be generated by this wealth of data: the long history of using star clusters to understand stars and galaxies is far from complete.

Acknowledgments

The authors thank the referee for their useful suggestions, and Marina Kounkel for helpful discussion. C.U. acknowledges the support of the Swedish Research Council, Vetenskapsrådet. K.C.D. acknowledges fellowship funding from Fonds de Recherche du Québec—Nature et Technologies, Bourses de recherche postdoctorale B3X no. 319864. L.G. acknowledges funding by an INAF Theory Grant 2022. P.B. acknowledges funding from an NSERC Discovery Grant. A.C.S. acknowledges funding from CNPq-314301/2021-6. W.I.C. gratefully acknowledges support from the Preparing for Astrophysics with LSST Program, funded by the Heising Simons Foundation through grant 2021-2975, and administered by Las Cumbres Observatory. M.G. gratefully acknowledges support by ANID/Fondecyt Project 1220724. A.P. acknowledges support from CNPq (Conselho Nacional de Desenvolvimento Científico e Tecnológico) Brazilian agency. R.A.S. gratefully acknowledges support from the National Science Foundation under grant No. 2206828. R.S.z. acknowledges the support by the Lendület Program of the Hungarian Academy of Sciences, project No. LP2018-7/2022. L.V. is supported by the National Aeronautics and Space Administration (NASA) under grant No. 80NSSC21K0633 issued through the NNH20ZDA001N Astrophysics Data Analysis Program (ADAP). M.R.C. gratefully acknowledges the Canadian Institute for Theoretical Astrophysics (CITA) National Fellowship for partial support; this work was supported by the Natural Sciences and Engineering Research Council of Canada (NSERC). E.A.H. acknowledges support from CAPES and CNPq.

ORCID iDs

Christopher Usher  <https://orcid.org/0000-0002-7383-7106>
 Kristen C. Dage  <https://orcid.org/0000-0002-8532-4025>
 Léo Girardi  <https://orcid.org/0000-0002-6301-3269>
 Pauline Barmby  <https://orcid.org/0000-0003-2767-0090>
 Charles J. Bonatto  <https://orcid.org/0000-0002-4102-1705>
 Ana L. Chies-Santos  <https://orcid.org/0000-0003-3220-0165>
 William I. Clarkson  <https://orcid.org/0000-0002-2577-8885>
 Matias Gómez Camus  <https://orcid.org/0000-0002-4430-9427>
 Eduardo A. Hartmann  <https://orcid.org/0000-0002-2527-8223>

Annette M. N. Ferguson  <https://orcid.org/0000-0001-7934-1278>
 Adriano Pieres  <https://orcid.org/0000-0001-9186-6042>
 Loredana Prisinzano  <https://orcid.org/0000-0002-8893-2210>
 Katherine L. Rhode  <https://orcid.org/0000-0001-8283-4591>
 Vincenzo Ripepi  <https://orcid.org/0000-0003-1801-426X>
 Keivan G. Stassun  <https://orcid.org/0000-0002-3481-9052>
 R. A. Street  <https://orcid.org/0000-0001-6279-0552>
 Róbert Szabó  <https://orcid.org/0000-0002-3258-1909>
 Laura Venuti  <https://orcid.org/0000-0002-4115-0318>
 Simone Zaggia  <https://orcid.org/0000-0001-6081-379X>
 Marco Canossa  <https://orcid.org/0000-0002-1261-1015>
 Pedro Floriano  <https://orcid.org/0009-0008-4034-7670>
 Pedro Lopes  <https://orcid.org/0009-0005-7299-4168>
 Nicole L. Miranda  <https://orcid.org/0009-0009-3088-5886>
 Raphael A. P. Oliveira  <https://orcid.org/0000-0002-4778-9243>
 Marta Reina-Campos  <https://orcid.org/0000-0002-8556-4280>
 A. Roman-Lopes  <https://orcid.org/0000-0002-1379-4204>
 Jennifer Sobeck  <https://orcid.org/0000-0002-4989-0353>

References

- Adamo, A., Hollyhead, K., Messa, M., et al. 2020, *MNRAS*, 499, 3267
 Adamo, A., Kruijssen, J. M. D., Bastian, N., Silva-Villa, E., & Ryon, J. 2015, *MNRAS*, 452, 246
 Adamo, A., Östlin, G., Zackrisson, E., et al. 2010, *MNRAS*, 407, 870
 Agüena, M., Benoist, C., da Costa, L. N., et al. 2021, *MNRAS*, 502, 4435
 Athukoralalage, W. R., Dage, K. C., Zepf, S. E., et al. 2023, *MNRAS*, 518, 855
 Balbinot, E., Santiago, B. X., da Costa, L., et al. 2013, *ApJ*, 767, 101
 Baldassare, V. F., Stone, N. C., Foord, A., Gallo, E., & Ostriker, J. P. 2022, *ApJ*, 929, 84
 Ballesteros-Paredes, J., Klessen, R. S., Mac Low, M. M., & Vazquez-Semadeni, E. 2007, in *Protostars and Planets V*, ed. B. Reipurth, D. Jewitt, & K. Keil (Tucson, AZ: Univ. Arizona Press), 63
 Bar, N., Blas, D., Blum, K., & Kim, H. 2021, *PhRvD*, 104, 043021
 Barbisan, E., Huang, J., Dage, K. C., et al. 2022, *MNRAS*, 514, 943
 Bastian, N., & Lardo, C. 2018, *ARA&A*, 56, 83
 Bastian, N., Pfeffer, J., Kruijssen, J. M. D., et al. 2020, *MNRAS*, 498, 1050
 Baumgardt, H., & Vasiliev, E. 2021, *MNRAS*, 505, 5957
 Bechtol, K., Drlica-Wagner, A., Balbinot, E., et al. 2015, *ApJ*, 807, 50
 Bell, C. P. M., Murphy, S. J., & Mamajek, E. E. 2017, *MNRAS*, 468, 1198
 Bellini, A., Libralato, M., Anderson, J., et al. 2019, arXiv:1903.05085
 Bianchini, P., Ibata, R., & Famaey, B. 2019, *ApJL*, 887, L12
 Bianchini, P., Renaud, F., Gieles, M., & Varri, A. L. 2015, *MNRAS*, 447, L40
 Bianco, F. B., Ivezić, Ž., Jones, R. L., et al. 2022, *ApJS*, 258, 1
 Bica, E., Bonatto, C., Dutra, C. M., & Santos, J. F. 2008, *MNRAS*, 389, 678
 Bica, E., Westera, P., Kerber, L. d. O., et al. 2020, *AJ*, 159, 82
 Blakeslee, J. P., Cho, H., Peng, E. W., et al. 2012, *ApJ*, 746, 88
 Blakeslee, J. P., Tonry, J. L., & Metzger, M. R. 1997, *AJ*, 114, 482
 Bonito, R., Venuti, L., Ustamujic, S., et al. 2023, *ApJS*, 265, 27
 Bouvier, J., Cabrit, S., Fernandez, M., Martin, E. L., & Mathews, J. M. 1993, *A&A*, 272, 176
 Bouvier, J., Matt, S. P., Mohanty, S., et al. 2014, in *Protostars and Planets VI*, ed. H. Beuther et al. (Tucson, AZ: Univ. Arizona Press), 433
 Brandt, T. D., & Huang, C. X. 2015, *ApJ*, 807, 24
 Brodie, J. P., & Larsen, S. S. 2002, *AJ*, 124, 1410
 Brodie, J. P., Romanowsky, A. J., Strader, J., et al. 2014, *ApJ*, 796, 52
 Brogaard, K., Grundahl, F., Sandquist, E. L., et al. 2021, *A&A*, 649, A178
 Brüns, R. C., & Kroupa, P. 2012, *A&A*, 547, A65
 Bullock, J. S., & Johnston, K. V. 2005, *ApJ*, 635, 931
 Caldwell, N., Strader, J., Romanowsky, A. J., et al. 2014, *ApJL*, 787, L11
 Calvet, N., & Gullbring, E. 1998, *ApJ*, 509, 802
 Calzetti, D., Lee, J. C., Sabbi, E., et al. 2015, *AJ*, 149, 51
 Cantat-Gaudin, T. 2022, *Univ*, 8, 111
 Cantat-Gaudin, T., Fouesneau, M., Rix, H.-W., et al. 2023, *A&A*, 669, A55
 Cantat-Gaudin, T., Jordi, C., Vallenari, A., et al. 2018, *A&A*, 618, A93
 Cantiello, M., & Blakeslee, J. P. 2007, *ApJ*, 669, 982
 Cantiello, M., Grado, A., Rejkuba, M., et al. 2018, *A&A*, 611, A21
 Carlsten, S. G., Greene, J. E., Beaton, R. L., & Greco, J. P. 2022, *ApJ*, 927, 44
 Carretta, E., Bragaglia, A., Gratton, R. G., et al. 2009, *A&A*, 505, 117
 Castro-Ginard, A., Jordi, C., Luri, X., et al. 2020, *A&A*, 635, A45
 Chadayammuri, U., Bogdán, Á., Oppenheimer, B. D., et al. 2022, *ApJL*, 936, L15
 Chandar, R., Bianchi, L., & Ford, H. C. 2000, *AJ*, 120, 3088
 Chandar, R., Fall, S. M., Whitmore, B. C., & Mulia, A. J. 2017, *ApJ*, 849, 128
 Chandar, R., Puzia, T. H., Sarajedini, A., & Goudfrooij, P. 2006, *ApJL*, 646, L107
 Chen, Y., Girardi, L., Fu, X., et al. 2019, *A&A*, 632, A105
 Chies-Santos, A. L., Cortesi, A., Fantin, D. S. M., et al. 2013, *A&A*, 559, A67
 Chies-Santos, A. L., de Souza, R. S., Caso, J. P., et al. 2022, *MNRAS*, 516, 1320
 Chies-Santos, A. L., Larsen, S. S., Cantiello, M., et al. 2012, *A&A*, 539, A54
 Chies-Santos, A. L., Larsen, S. S., Kuntschner, H., et al. 2011, *A&A*, 525, A20
 Choi, J., Dotter, A., Conroy, C., et al. 2016, *ApJ*, 823, 102
 Choksi, N., & Gnedin, O. Y. 2019, *MNRAS*, 488, 5409
 Claeysens, A., Adamo, A., Richard, J., et al. 2023, *MNRAS*, 520, 2180
 Conroy, C., & Gunn, J. E. 2010, *ApJ*, 712, 833
 Conroy, C., Gunn, J. E., & White, M. 2009, *ApJ*, 699, 486
 Cordoni, G., Milone, A. P., Marino, A. F., et al. 2018, *ApJ*, 869, 139
 Correnti, M., Goudfrooij, P., Bellini, A., & Girardi, L. 2021, *MNRAS*, 504, 155
 Correnti, M., Goudfrooij, P., Bellini, A., Kalirai, J. S., & Puzia, T. H. 2017, *MNRAS*, 467, 3628
 Costa, G., Girardi, L., Bressan, A., et al. 2019, *MNRAS*, 485, 4641
 Costigan, G., Vink, J. S., Scholz, A., Ray, T., & Testi, L. 2014, *MNRAS*, 440, 3444
 Cote, P., Abraham, B., Balogh, M., et al. 2019, CASTOR: A Flagship Canadian Space Telescope, Zenodo, doi:10.5281/zenodo.3758463
 Côté, P., Blakeslee, J. P., Ferrarese, L., et al. 2004, *ApJS*, 153, 223
 Crnojević, D., Sand, D. J., Zaritsky, D., et al. 2016, *ApJL*, 824, L14
 Culpan, R., Geier, S., Reindl, N., et al. 2022, *A&A*, 662, A40
 Cummings, J. D., Kalirai, J. S., Tremblay, P. E., Ramirez-Ruiz, E., & Choi, J. 2018, *ApJ*, 866, 21
 Da Costa, G. S. 1991, in *The Magellanic Clouds in IAU Symp. 148*, ed. R. Haynes & D. Milne (Dordrecht: Kluwer), 183
 Dage, K. C., Kundu, A., Thygesen, E., et al. 2021, *MNRAS*, 504, 1545
 Dage, K. C., Zepf, S. E., Thygesen, E., et al. 2020, *MNRAS*, 497, 596
 Dal Tio, P., Pastorelli, G., Mazzi, A., et al. 2022, *ApJS*, 262, 22
 Dalgleish, H., Kamann, S., Usher, C., et al. 2020, *MNRAS*, 492, 3859
 Damiani, F. 2018, *A&A*, 615, A148
 de Boer, T. J. L., Gieles, M., Balbinot, E., et al. 2019, *MNRAS*, 485, 4906
 Deason, A. J., Wetzel, A. R., Garrison-Kimmel, S., & Belokurov, V. 2015, *MNRAS*, 453, 3568
 Delgado, F., Saha, A., Chandrasekharan, S., et al. 2014, *Proc. SPIE*, 9150, 915015
 Di Carlo, U. N., Mapelli, M., Pasquato, M., et al. 2021, *MNRAS*, 507, 5132
 Dias, B., Kerber, L., Barbuy, B., Bica, E., & Ortolani, S. 2016, *A&A*, 591, A11
 Dias, B., Maia, F., Kerber, L., et al. 2020, in *Star Clusters: From the Milky Way to the Early Universe in IAU Symp. 351*, ed. A. Bragaglia et al. (Cambridge: Cambridge Univ. Press), 89
 Dias, B., Parisi, M. C., Angelo, M., et al. 2022, *MNRAS*, 512, 4334
 Dirsch, B., Richtler, T., Geisler, D., et al. 2003, *AJ*, 125, 1908
 Dotter, A. 2016, *ApJS*, 222, 8
 Dotter, A., Sarajedini, A., & Yang, S.-C. 2008, *AJ*, 136, 1407
 Doyle, T. F., Shara, M. M., Lessing, A. M., & Zurek, D. 2019, *ApJ*, 874, 65
 Driver, S. P., Bellstedt, S., Robotham, A. S. G., et al. 2022, *MNRAS*, 513, 439
 Eadie, G. M., Harris, W. E., & Springford, A. 2022, *ApJ*, 926, 162

- Ekström, S., Georgy, C., Eggenberger, P., et al. 2012, *A&A*, **537**, A146
- El-Badry, K., Quataert, E., Weisz, D. R., Choksi, N., & Boylan-Kolchin, M. 2019, *MNRAS*, **482**, 4528
- Elmegreen, B. G. 2010, *ApJL*, **712**, L184
- Elmegreen, B. G., & Efremov, Y. N. 1997, *ApJ*, **480**, 235
- Elson, R. A. W. 1991, *ApJS*, **76**, 185
- Elson, R. A. W., Freeman, K. C., & Lauer, T. R. 1989, *ApJL*, **347**, L69
- Fadely, R., Hogg, D. W., & Willman, B. 2012, *ApJ*, **760**, 15
- Fahion, K., Lyubenova, M., Hilker, M., et al. 2020, *A&A*, **637**, A27
- Farrell, S. A., Servillat, M., Pforr, J., et al. 2012, *ApJL*, **747**, L13
- Farrell, S. A., Webb, N. A., Barret, D., Godet, O., & Rodrigues, J. M. 2009, *Natur*, **460**, 73
- Ferraro, F. R., Dalessandro, E., Mucciarelli, A., et al. 2009, *Natur*, **462**, 483
- Ferraro, F. R., Pallanca, C., Lanzoni, B., et al. 2021, *NatAs*, **5**, 311
- Fischer, W. J., Hillenbrand, L. A., Herczeg, G. J., et al. 2022, arXiv:2203.11257
- Flaischlen, S., Preibisch, T., Kluge, M., Manara, C. F., & Ercolano, B. 2022, *A&A*, **666**, A55
- Forbes, D. A., Alabi, A., Romanowsky, A. J., et al. 2016, *MNRAS*, **458**, L44
- Forbes, D. A., & Bridges, T. 2010, *MNRAS*, **404**, 1203
- Forbes, D. A., Read, J. I., Gieles, M., & Collins, M. L. M. 2018, *MNRAS*, **481**, 5592
- Frogel, J. A., Mould, J., & Blanco, V. M. 1990, *ApJ*, **352**, 96
- Gaia Collaboration, Babusiaux, C., van Leeuwen, F., et al. 2018, *A&A*, **616**, A10
- Gatto, M., Ripepi, V., Bellazzini, M., et al. 2020, *MNRAS*, **499**, 4114
- Gatto, M., Ripepi, V., Bellazzini, M., et al. 2021, *MNRAS*, **507**, 3312
- Gatto, M., Ripepi, V., Bellazzini, M., et al. 2022, *A&A*, **664**, L12
- Geier, S., Raddi, R., Gentile, F. N. P., & Marsh, T. R. 2019, *A&A*, **621**, A38
- Geller, A. M., Polzin, A., Bowen, A., & Miller, A. A. 2021, *ApJ*, **919**, 83
- Georgiev, I. Y., Goudfrooij, P., & Puzia, T. H. 2012, *MNRAS*, **420**, 1317
- Gillen, E., Hillenbrand, L. A., Stauffer, J., et al. 2020, *MNRAS*, **495**, 1531
- Girardi, L., Boyer, M. L., Johnson, L. C., et al. 2020, *ApJ*, **901**, 19
- Girardi, L., Costa, G., Chen, Y., et al. 2019, *MNRAS*, **488**, 696
- Girardi, L., Rubele, S., & Kerber, L. 2009, *MNRAS*, **394**, L74
- Goddard, Q. E., Bastian, N., & Kennicutt, R. C. 2010, *MNRAS*, **405**, 857
- Gossage, S., Conroy, C., Dotter, A., et al. 2018, *ApJ*, **863**, 67
- Gratton, R., Bragaglia, A., Carretta, E., et al. 2019, *A&ARv*, **27**, 8
- Gullbring, E., Hartmann, L., Briceño, C., & Calvet, N. 1998, *ApJ*, **492**, 323
- Guy, L. P., Cuillandre, J.-C., Bachelet, E., et al. 2022, Rubin-Euclid Derived Data Products: Initial Recommendations, Zenodo, doi:10.5281/zenodo.5836022
- Hambleton, K. M., Bianco, F. B., Street, R., et al. 2022, arXiv:2208.04499
- Hao, C. J., Xu, Y., Wu, Z. Y., et al. 2022, *A&A*, **660**, A4
- Harris, W. E. 1996, *AJ*, **112**, 1487
- Harris, W. E. 2001, in Saas-Fee Advanced Course 28: Star Clusters, ed. L. Labhardt & B. Binggeli (Berlin: Springer), 223
- Harris, W. E. 2009, *ApJ*, **699**, 254
- Harris, W. E., Brown, R. A., Durrell, P. R., et al. 2020, *ApJ*, **890**, 105
- Hartmann, E. A., Bonatto, C. J., Chies-Santos, A. L., et al. 2022, *MNRAS*, **515**, A191
- Hartmann, L., Herczeg, G., & Calvet, N. 2016, *ARA&A*, **54**, 135
- Heber, U. 2009, *ARA&A*, **47**, 211
- Hillenbrand, L. A., & White, R. J. 2004, *ApJ*, **604**, 741
- Hodge, P. W., Dolphin, A. E., Smith, T. R., & Mateo, M. 1999, *ApJ*, **521**, 577
- Holtzman, J. A., Watson, A. M., Mould, J. R., et al. 1996, *AJ*, **112**, 416
- Hudson, M. J., Harris, G. L., & Harris, W. E. 2014, *ApJL*, **787**, L5
- Hughes, A. K., Sand, D. J., Seth, A., et al. 2021, *ApJ*, **914**, 16
- Hughes, M. E., Jethwa, P., Hilker, M., et al. 2021, *MNRAS*, **502**, 2828
- Hunt, E. L., & Reffert, S. 2021, *A&A*, **646**, A104
- Hunt, E. L., & Reffert, S. 2023, *A&A*, **673**, A114
- Hunt, Q., Gallo, E., Chandar, R., Mok, A., & Prestwich, A. 2023, *ApJ*, **947**, 31
- Huxor, A. P., Mackey, A. D., Ferguson, A. M. N., et al. 2014, *MNRAS*, **442**, 2165
- Huxor, A. P., Tanvir, N. R., Irwin, M. J., et al. 2005, *MNRAS*, **360**, 1007
- Ibata, R. A., Bellazzini, M., Malhan, K., Martin, N., & Bianchini, P. 2019, *NatAs*, **3**, 667
- Ireland, L. G., Zanni, C., Matt, S. P., & Pantolmos, G. 2021, *ApJ*, **906**, 4
- Ivezić, Ž., Kahn, S. M., Tyson, J. A., et al. 2019, *ApJ*, **873**, 111
- Jadhav, V. V., & Subramaniam, A. 2021, *MNRAS*, **507**, 1699
- Jensen, J. B., Blakeslee, J. P., Gibson, Z., et al. 2015, *ApJ*, **808**, 91
- Jethwa, P., Erkal, D., & Belokurov, V. 2016, *MNRAS*, **461**, 2212
- Johnson, C. I., Rich, R. M., Young, M. D., et al. 2020, *MNRAS*, **499**, 2357
- Jones, M. G., Karunakaran, A., Bennet, P., et al. 2023, *ApJL*, **942**, L5
- Jones, R. L., Joachim, P., Chandrasekharan, S., et al. 2014, *Proc. SPIE*, **9149**, 91490B
- Jordán, A., Blakeslee, J. P., Côté, P., et al. 2007a, *ApJS*, **169**, 213
- Jordán, A., McLaughlin, D. E., Côté, P., et al. 2007b, *ApJS*, **171**, 101
- Kamann, S., Peng, E. W., Blakeslee, J. P., et al. 2009, *ApJS*, **180**, 54
- Kader, J. A., Pilachowski, C. A., Johnson, C. I., et al. 2022, *ApJ*, **940**, 76
- Kalari, V. M., Vink, J. S., Drew, J. E., et al. 2015, *MNRAS*, **453**, 1026
- Kamann, S., Bastian, N., Gossage, S., et al. 2020, *MNRAS*, **492**, 2177
- Kamann, S., Bastian, N., Usher, C., Cabrera-Ziri, I., & Saracino, S. 2021, *MNRAS*, **508**, 2302
- Kamann, S., Bastian, N. J., Gieles, M., Balbinot, E., & Hénault-Brunet, V. 2019, *MNRAS*, **483**, 2197
- Kamann, S., Saracino, S., Bastian, N., et al. 2023, *MNRAS*, **518**, 1505
- Kang, J., Lee, M. G., Jang, I. S., et al. 2022, *ApJ*, **939**, 74
- Kato, M., Hachisu, I., & Henze, M. 2013, *ApJ*, **779**, 19
- Kharchenko, N. V., Piskunov, A. E., Schilbach, E., Röser, S., & Scholz, R. D. 2013, *A&A*, **558**, A53
- King, I. 1962, *AJ*, **67**, 471
- Kirsten, F., Marcote, B., Nimmo, K., et al. 2022, *Natur*, **602**, 585
- Kissler-Patig, M., Brodie, J. P., & Minniti, D. 2002, *A&A*, **391**, 441
- Koposov, S. E., Belokurov, V., Torrealba, G., & Evans, N. W. 2015, *ApJ*, **805**, 130
- Kounkel, M., Covey, K., & Stassun, K. G. 2020, *AJ*, **160**, 279
- Kounkel, M., Stassun, K. G., Bouma, L. G., et al. 2022, *AJ*, **164**, 137
- Krienke, K., & Hodge, P. 2004, *PASP*, **116**, 497
- Kruijssen, J. M. D. 2015, *MNRAS*, **454**, 1658
- Kruijssen, J. M. D., Pfeffer, J. L., Chevance, M., et al. 2020, *MNRAS*, **498**, 2472
- Kruijssen, J. M. D., Pfeffer, J. L., Crain, R. A., & Bastian, N. 2019, *MNRAS*, **486**, 3134
- Kruijssen, J. M. D., Schruha, A., Hygate, A. P. S., et al. 2018, *MNRAS*, **479**, 1866
- Kuzma, P. B., Ferguson, A. M. N., & Peñarrubia, J. 2021, *MNRAS*, **507**, 1127
- Lada, C. J. 2006, *ApJL*, **640**, L63
- Lada, C. J., & Lada, E. A. 2003, *ARA&A*, **41**, 57
- Lardo, C., Bellazzini, M., Pancino, E., et al. 2011, *A&A*, **525**, A114
- Larsen, S. S. 2009, *A&A*, **494**, 539
- Larsen, S. S., & Richtler, T. 2000, *A&A*, **354**, 836
- Lee, J. C., Whitmore, B. C., Thilker, D. A., et al. 2022, *ApJS*, **258**, 10
- Lee, S.-Y., Chung, C., & Yoon, S.-J. 2019, *ApJS*, **240**, 2
- Lehmer, B. D., Ferrell, A. P., Doore, K., et al. 2020, *ApJS*, **248**, 31
- Leiner, E. M., & Geller, A. 2021, *ApJ*, **908**, 229
- Leitinger, E., Baumgardt, H., Cabrera-Ziri, I., Hilker, M., & Pancino, E. 2023, *MNRAS*, **520**, 1456
- Li, D. D., Eadie, G. M., Abraham, R., et al. 2022, *ApJ*, **935**, 3
- Li, H., & Gnedin, O. Y. 2014, *ApJ*, **796**, 10
- Liu, B., Ormel, C. W., & Lin, D. N. C. 2017, *A&A*, **601**, A15
- LSST Science Collaboration, Abell, P. A., Allison, J., et al. 2009, arXiv:0912.0201
- Luhman, K. L. 2012, *ARA&A*, **50**, 65
- Maccarone, T. J., Kundu, A., Zepf, S. E., & Rhode, K. L. 2007, *Natur*, **445**, 183
- Mackey, A. D., Broby Nielsen, P., Ferguson, A. M. N., & Richardson, J. C. 2008, *ApJL*, **681**, L17
- Mackey, A. D., Ferguson, A. M. N., Huxor, A. P., et al. 2019, *MNRAS*, **484**, 1756
- Mackey, A. D., & Gilmore, G. F. 2003, *MNRAS*, **338**, 120
- Maia, F. F. S., Dias, B., Santos, J. F. C., et al. 2019, *MNRAS*, **484**, 5702
- Mapelli, M., & Zampieri, L. 2014, *ApJ*, **794**, 7
- Marconi, M., Molinaro, R., Ripepi, V., Musella, I., & Brocato, E. 2013, *MNRAS*, **428**, 2185
- Marigo, P., Bossini, D., Trabucchi, M., et al. 2022, *ApJS*, **258**, 43
- Marigo, P., Cummings, J. D., Curtis, J. L., et al. 2020, *NatAs*, **4**, 1102
- Martell, S. L., Smolinski, J. P., Beers, T. C., & Grebel, E. K. 2011, *A&A*, **534**, A136
- Martens, S., Kamann, S., Dreizler, S., et al. 2023, *A&A*, **671**, A106

- Martocchia, S., Bastian, N., Saracino, S., & Kamann, S. 2023, *MNRAS*, **520**, 4080
- Massana, P., Ruiz-Lara, T., Noël, N. E. D., et al. 2022, *MNRAS*, **513**, L40
- Masters, K. L., Jordán, A., Côté, P., et al. 2010, *ApJ*, **715**, 1419
- Mau, S., Drlica-Wagner, A., Bechtol, K., et al. 2019, *ApJ*, **875**, 154
- McBride, A., Lingg, R., Kounkel, M., Covey, K., & Hutchinson, B. 2021, *AJ*, **162**, 282
- Mei, S., Blakeslee, J. P., Côté, P., et al. 2007, *ApJ*, **655**, 144
- Meibom, S., Grundahl, F., Clausen, J. V., et al. 2009, *AJ*, **137**, 5086
- Milone, A. P., Bedin, L. R., Piotto, G., & Anderson, J. 2009, *A&A*, **497**, 755
- Milone, A. P., Cordonì, G., Marino, A. F., et al. 2022, arXiv:2212.07978
- Milone, A. P., Marino, A. F., D'Antona, F., et al. 2016, *MNRAS*, **458**, 4368
- Mohammadi, M., Mutatiina, J., Saifollahi, T., & Bunte, K. 2022, *A&C*, **39**, 100555
- Mora, M. D., Larsen, S. S., & Kissler-Patig, M. 2008, *A&A*, **489**, 1065
- Mowla, L., Iyer, K. G., Desprez, G., et al. 2022, *ApJL*, **937**, L35
- Muñoz, R. P., Puzia, T. H., Lançon, A., et al. 2014, *ApJS*, **210**, 4
- Musella, I., Ripepi, V., Brocato, E., et al. 2006, *MmSAI*, **77**, 291
- Nardiello, D., Libralato, M., Piotto, G., et al. 2018, *MNRAS*, **481**, 3382
- Neumayer, N., Seth, A., & Böker, T. 2020, *A&ARv*, **28**, 4
- Offner, S. S. R., Clark, P. C., Hennebelle, P., et al. 2014, in *Protostars and Planets VI*, ed. H. Beuther et al. (Tucson, AZ: Arizona Univ. Press), **53**
- Origlia, L., Rich, R. M., Ferraro, F. R., et al. 2011, *ApJL*, **726**, L20
- Pace, A. B., Walker, M. G., Kozlov, S. E., et al. 2021, *ApJ*, **923**, 77
- Palla, F., Randich, S., Flaccomio, E., & Pallavicini, R. 2005, *ApJL*, **626**, L49
- Parisi, M. C., Geisler, D., Carraro, G., et al. 2014, *AJ*, **147**, 71
- Patel, E., Kallivayalil, N., Garavito-Camargo, N., et al. 2020, *ApJ*, **893**, 121
- Peacock, M. B., Zepf, S. E., Kundu, A., et al. 2017, *ApJ*, **841**, 28
- Peebles, P. J. E. 1984, *ApJ*, **277**, 470
- Peltonen, J., Rosolowsky, E., Johnson, L. C., et al. 2023, *MNRAS*, **522**, 6137
- Peng, E. W., Côté, P., Jordán, A., et al. 2006, *ApJ*, **639**, 838
- Pérez, G., Messa, M., Calzetti, D., et al. 2021, *ApJ*, **907**, 100
- Pfeffer, J., Kruijssen, J. M. D., Crain, R. A., & Bastian, N. 2018, *MNRAS*, **475**, 4309
- Pfeffer, J. L., Trujillo-Gomez, S., Kruijssen, J. M. D., et al. 2020, *MNRAS*, **499**, 4863
- Piatti, A. E. 2022, *MNRAS*, **511**, L72
- Piotto, G., Milone, A. P., Bedin, L. R., et al. 2015, *AJ*, **149**, 91
- Powalka, M., et al. 2016, *ApJL*, **829**, L5
- Prisinzano, L., Bonito, R., Mazzi, A., et al. 2023, *ApJS*, **265**, 39
- Prisinzano, L., Damiani, F., Guarcello, M. G., et al. 2018, *A&A*, **617**, A63
- Prisinzano, L., Damiani, F., Sciortino, S., et al. 2022, *A&A*, **664**, A175
- Qu, H., Yuan, Z., Doliva-Dolinsky, A., et al. 2023, *MNRAS*, **523**, 876
- Rain, M. J., Ahumada, J. A., & Carraro, G. 2021, *A&A*, **650**, A67
- Rangelov, B., Chandar, R., Prestwich, A., & Whitmore, B. C. 2012, *ApJ*, **758**, 99
- Rastello, S., Mapelli, M., Di Carlo, U. N., et al. 2020, *MNRAS*, **497**, 1563
- Rastello, S., Mapelli, M., Di Carlo, U. N., et al. 2021, *MNRAS*, **507**, 3612
- Reina-Campos, M., Trujillo-Gomez, S., Deason, A. J., et al. 2021, arXiv:2106.07652
- Rejkuba, M. 2012, *Astrophysics and Space Science*, **341**, 195
- Rhode, K. L., & Zepf, S. E. 2004, *AJ*, **127**, 302
- Ribas, Á., Merín, B., Bouy, H., & Maud, L. T. 2014, *A&A*, **561**, A54
- Rich, R. M., Johnson, C. I., Young, M., et al. 2020, *MNRAS*, **499**, 2340
- Riess, A. G., Breuval, L., Yuan, W., et al. 2022, *ApJ*, **938**, 36
- Rigliaco, E., Natta, A., Randich, S., Testi, L., & Biazzo, K. 2011, *A&A*, **525**, A47
- Rodríguez, C. L., Hafen, Z., Grudić, M. Y., et al. 2023, *MNRAS*, **521**, 124
- Romanova, M. M., Lii, P. S., Koldoba, A. V., et al. 2019, *MNRAS*, **485**, 2666
- Romanowsky, A. J., Larsen, S. S., Villaume, A., et al. 2023, *MNRAS*, **518**, 3164
- Sánchez-Janssen, R., Côté, P., Ferrarese, L., et al. 2019, *ApJ*, **878**, 18
- Sánchez-Salcedo, F. J., & Lora, V. 2022, *MNRAS*, **511**, 1860
- Sarajedini, A., Bedin, L. R., Chaboyer, B., et al. 2007, *AJ*, **133**, 1658
- Schiavon, R. P., Zamora, O., Carrera, R., et al. 2017, *MNRAS*, **465**, 501
- Senchyna, P., Johnson, L. C., Dalcanton, J. J., et al. 2015, *ApJ*, **813**, 31
- Sharina, M. E., Afanasiev, V. L., & Puzia, T. H. 2006, *MNRAS*, **372**, 1259
- Siess, L., Dufour, E., & Forestini, M. 2000, *A&A*, **358**, 593
- Silva-Villa, E., & Larsen, S. S. 2011, *A&A*, **529**, A25
- Slater, C. T., Ivezić, Ž., & Lupton, R. H. 2020, *AJ*, **159**, 65
- Sollima, A. 2020, *MNRAS*, **495**, 2222
- Spitler, L. R., & Forbes, D. A. 2009, *MNRAS*, **392**, L1
- Stassun, K., & Wood, K. 1999, *ApJ*, **510**, 892
- Stassun, K. G., Collins, K. A., & Gaudi, B. S. 2017, *AJ*, **153**, 136
- Stassun, K. G., Corsaro, E., Pepper, J. A., & Gaudi, B. S. 2018, *AJ*, **155**, 22
- Stassun, K. G., Mathieu, R. D., & Valenti, J. A. 2006, *Natur*, **440**, 311
- Stassun, K. G., & Torres, G. 2016, *AJ*, **152**, 180
- Stassun, K. G., Torres, G., Kounkel, M., et al. 2022, *ApJ*, **941**, 125
- Stassun, K. G., Torres, G., Kounkel, M., et al. 2023, arXiv:2305.00134
- Stetson, P. B., Pancino, E., Zocchi, A., Sanna, N., & Monelli, M. 2019, *MNRAS*, **485**, 3042
- Stone, N. C., Küpper, A. H. W., & Ostriker, J. P. 2017, *MNRAS*, **467**, 4180
- Strader, J., Caldwell, N., & Seth, A. C. 2011, *AJ*, **142**, 8
- Tassis, K., & Mouschovias, T. C. 2004, *ApJ*, **616**, 283
- Taylor, M. A., Puzia, T. H., Muñoz, R. P., et al. 2017, *MNRAS*, **469**, 3444
- Thilker, D. A., Whitmore, B. C., Lee, J. C., et al. 2022, *MNRAS*, **509**, 4094
- Thompson, I. B., Kaluzny, J., Rucinski, S. M., et al. 2010, *AJ*, **139**, 329
- Tremaine, S. D. 1976, *ApJ*, **203**, 345
- Trenti, M., Padoan, P., & Jimenez, R. 2015, *ApJL*, **808**, L35
- Tudorica, A., Georgiev, I. Y., & Chies-Santos, A. L. 2015, *A&A*, **581**, A84
- Udalski, A., Szymański, M. K., & Szymański, G. 2015, *AcA*, **65**, 1
- Usher, C., Beckwith, T., Bellstedt, S., et al. 2019a, *MNRAS*, **482**, 1275
- Usher, C., Brodie, J. P., Forbes, D. A., et al. 2019b, *MNRAS*, **490**, 491
- Usher, C., Forbes, D. A., Brodie, J. P., et al. 2012, *MNRAS*, **426**, 1475
- Usher, C., Forbes, D. A., Brodie, J. P., et al. 2015, *MNRAS*, **446**, 369
- Valenzuela, L. M., Moster, B. P., Remus, R.-S., O'Leary, J. A., & Burkert, A. 2021, *MNRAS*, **505**, 5815
- Veljanoski, J., Ferguson, A. M. N., Mackey, A. D., et al. 2015, *MNRAS*, **452**, 320
- Veljanoski, J., Mackey, A. D., Ferguson, A. M. N., et al. 2014, *MNRAS*, **442**, 2929
- Venuti, L., Bouvier, J., Flaccomio, E., et al. 2014, *A&A*, **570**, A82
- Venuti, L., Bouvier, J., Irwin, J., et al. 2015, *A&A*, **581**, A66
- Venuti, L., Cody, A. M., Rebull, L. M., et al. 2021, *AJ*, **162**, 101
- Venuti, L., Damiani, F., & Prisinzano, L. 2019, *A&A*, **621**, A14
- Villegas, D., Jordán, A., Peng, E. W., et al. 2010, *ApJ*, **717**, 603
- Voggel, K. T., Seth, A. C., Sand, D. J., et al. 2020, *ApJ*, **899**, 140
- Voss, R., & Nelemans, G. 2012, *A&A*, **539**, A77
- Vrba, F. J., Chugainov, P. F., Weaver, W. B., & Stauffer, J. S. 1993, *AJ*, **106**, 1608
- Wainer, T. M., Johnson, L. C., Seth, A. C., et al. 2022, *ApJ*, **928**, 15
- Wang, C., Langer, N., Schootemeijer, A., et al. 2020, *ApJL*, **888**, L12
- Washabaugh, P. C., & Bregman, J. N. 2013, *ApJ*, **762**, 1
- Weidemann, V. 2000, *A&A*, **363**, 647
- Welch, D. L., & Stetson, P. B. 1993, *AJ*, **105**, 1813
- Whitmore, B. C., Chandar, R., Rodríguez, M. J., et al. 2023, *ApJL*, **944**, L14
- Whitmore, B. C., & Schweizer, F. 1995, *AJ*, **109**, 960
- Wyder, T. K., Hodge, P. W., & Cole, A. 2000, *PASP*, **112**, 594
- Zanatta, E., Sánchez-Janssen, R., Chies-Santos, A. L., de Souza, R. S., & Blakeslee, J. P. 2021, *MNRAS*, **508**, 986
- Zaritsky, D. 2022, *MNRAS*, **513**, 2609